PNAS
www.pnas.org

# Supplementary Information for

## Bcl6 controls meningeal Th17-B cell interaction in murine neuroinflammation

Maike Hartlehnert[1,§], Anna-Lena Börsch[1,§], Xiaolin Li[1,§], Miriam Burmeister[2,3], Hanna Gerwien[2,3], David Schafflick[1], Michael Heming[1], I-Na Lu[1], Venu Narayanan[1], Jan-Kolja Strecker[1], Anna Kolz[4], Anneli Peters[4,5], Gregory F. Wu[6], Heinz Wiendl[1,3], Lydia Sorokin[2,3], and Gerd Meyer zu Horste[1,*]
§ These authors contributed equally

1) Department of Neurology with Institute of Translational Neurology, University Hospital Münster, Münster, Germany (48149)
2) Institute of Physiological Chemistry and Pathobiochemistry, University of Münster, Münster, Germany (48149)
3) Cells in Motion Interfaculty Centre, University of Münster, Münster, Germany (48149)
4) Institute of Clinical Neuroimmunology, University Hospital, LMU Munich, Munich, Germany (81377)
5) Biomedical Center (BMC), Faculty of Medicine, LMU Munich, Munich, Germany (81377)
6) Department of Neurology, Washington University in St. Louis, St. Louis, MO, USA.

*Corresponding author: Gerd Meyer zu Hörste
**Email:** gerd.meyerzuhoerste@ukmuenster.de

**This PDF file includes:**



**Other supplementary materials for this manuscript include the following:**

Datasets S1 to S26

**Supplementary Methods**

*Mice*

C57BL/6J, CD4$^{Cre}$ mice (1), C57BL/6-Tg(Tcra2D2,Tcrb2D2)1Kuch/J (named 2D2$^{tg}$) mice (2), and B6.129 S(FVB)-*Bcl6*$^{tm1.1Dent}$/J (named Bcl6$^{flox}$ or Bcl6$^{fl/fl}$) mice (3) were purchased from the Jackson laboratories. The breeding strategies of the CD4$^{Cre}$Bcl6$^{fl/fl}$2D2$^{tg}$ and CD4$^{Cre}$Bcl6$^{fl/fl}$ strains were described previously (4). Animal research protocols were approved by the responsible state authorities (Landesamt für Natur, Umwelt und Verbraucherschutz (LANUV), English: 'State Agency for Nature, Environment and Consumer Protection' of the German state North Rhine-Westphalia (NRW)) under reference number 84-02.04.2015.A319 and were performed in accordance with local regulations from the "Tierschutzbüro der Medizinischen Fakultät der Westfälischen Wilhelms-Universitat Münster" (English: Animal Protection Office of the Medical Faculty of the Westfälische Wilhelms-University Münster). Mice of both sexes were used (age 8-14 weeks). Igh-J$^{tm1Aigl}$ mice (synonymously named TH mice or IgH$^{MOG}$ mice; (5)) were used for B cell proliferation in *in vitro* experiments.

*Adoptive transfer (AT) experimental autoimmune encephalomyelitis (EAE) and active EAE*

Adoptive transfer EAE was induced as described (6). Briefly, naïve CD44$^{low}$CD62L$^{high}$ CD4$^{+}$ T cells were sorted from 2D2$^{tg}$ donor mice and cultured for 2 days at 2x10$^{6}$ cells/ml in the presence of irradiated antigen presenting cells in medium containing soluble anti-CD3 antibody (2.5 µg/ml), IL-6 (20 ng/ml), TGF-β1 (10 ng/ml) and anti-IFNγ antibody (10 µg/ml) (all cytokines from R&D). Cells were subsequently split when necessary and cultured in IL-23 (10 ng/ml) containing medium for 3 additional days. Cells were then resuspended in medium containing soluble anti-CD28 antibody (2 µg/ml) and plated at a concentration of 2x10$^{6}$ cells/ml on anti-CD3 (2 µg/ml) coated plates in the absence of cytokines for 2 days. 5x10$^{6}$ cells were then intravenously injected into young adult C57BL/6 recipient mice. Recipient mice were monitored daily and an ataxia score was calculated by assessing the following criteria: ledge test, hindlimb clasping, gait and kyphosis (7). Each criteria was rated on a scale from 0 (healthy) to 3 and all points were added up to a maximum ataxia score of 12 as described (4). Active EAE was induced with a subcutaneous injection of MOG$_{35-55}$ peptide (200 µg/mouse, Charité, Berlin) and Mycobacterium tuberculosis H37Ra extract (1 mg/ml, BD) in complete Freund's adjuvant (200 µl/mouse). EAE mice were clinically monitored as described previously (4).

*Leukocyte isolation from CNS*

Labeling of blood leukocytes to identify tissue-resident leukocytes (TRL) was performed by intravenous injection of fluorescence coupled anti-CD45.2 antibody (clone 104, Biolegend, 3 µg/mouse) into the tail vein of mice as described (8). Five minutes after antibody injection, animals were anesthetized with Ketamine / Xylazine and intracardially perfused with cold phosphate-buffered saline (PBS) with 10 U/ml heparin.

For separate isolation of the parenchymal and the meningeal tissue of the spinal cord (SC), SC parenchyma was flushed out from the spinal canal with hydrostatic pressure after removing the brain. The SC meninges remained attached to the vertebrae and were then peeled off the vertebrae under a binocular. Spinal nerves and ganglia were removed from meningeal tissue using fine forceps.

Parenchymal SC tissue was cut up and then digested with collagenase D (2.5 mg/ml, Roche Diagnostics) and DNase I (0.05 mg/ml, Sigma) for 20 min at 37 °C. Meningeal tissue was digested under continuous shaking in PBS with 1 mg/ml collagenase D for 45 min at 37°C. The digested tissue was passed through a 40 µm cell strainer. Parenchymal homogenates were layered on a 70% / 37% Percoll gradient and centrifuged as described (4). The interphase was removed and

washed and purified cells were subsequently stained for flow cytometry or fluorescence activated cell sorting (FACS) for scRNA-seq into FCS-coated tubes or for bulk RNA sequencing into RNA lysis buffer.

*Flow cytometry analysis and FACS*

Cells were stained for flow cytometry or FACS for 30 min at room temperature with anti-mouse antibodies (clone names in brackets, BioLegend unless indicated otherwise): CD45 (30-11 F), CD3 (17A2), CD4 (RM4-5 or GK1.5), TCR Vβ11 (KT11), CD19 (6D5), CD11b (M1/70); live/dead staining was performed with "Zombie NIR" (1:500). To quantify cytokine production, cells were resuspended in culture medium containing 20 ng/ml PMA, 500 ng/ml ionomycin, GolgiStop, and GolgiPlug (BD, each 1:1000 diluted). After 4 h of incubation at 37 °C, cells were stained extracellularly, fixed, and permeabilized using the Cytofix/Cytoperm kit (BD) according to the manufacturer's protocol. Then, IL-17A (eBioscience, eBio17B7) and IFN-γ (XMG1.2) were stained intracellularly. After staining, cells were washed twice and resuspended in MACS buffer (PBS with 0.5% BSA, 2mM EDTA, pH = 7.2). Cells were acquired using a Gallios (Beckman Coulter) flow cytometer, or a FACSCelesta flow cytometer (Becton Dickinson) or sorted on a BD FACS Aria III cell sorter using FACS Diva software following manufacturer's recommended settings. Sorting of viable tissue-resident leukocytes - either $CD45^{high}$ leukocytes or $V\beta11^{+}$ $CD4^{+}$ T cells - was performed using an 85 µm nozzle and the sort precision mode "purity". Flow cytometry data were analyzed using FlowJo software v10.7.0_CL.

*Single cell RNA-sequencing (scRNA-seq) - Generation of single cell libraries, sequencing, and preprocessing of sequencing data.*

Single cell suspensions were loaded onto the Chromium Single Cell Controller using the Chromium Single Cell 3' Library & Gel Bead Kit (both from 10X Genomics) with v3 chemistry. Sample processing and library preparation was performed according to manufacturer's instructions using AMPure beads (Beckman Coulter). In order to avoid batch effects, all four samples (Dataset S1) were processed on the same day with the same chip. The rest of cDNA was used for single cell TCR sequencing (see below). Sequencing was carried out commercially on an Illumina Novaseq with 150-8-8-150 read setup. Details regarding sequencing depth and cell recovery are provided in Dataset S1. Processing of sequencing data was performed with the *cellranger* pipeline v3.0.2 (10X Genomics) according to the manufacturer's instructions. Briefly, subsequent read alignments and transcript counting was done individually for each sample using the *cellranger count* pipeline with standard parameters. The *cellranger aggr* pipeline was employed to aggregate samples with mapping normalization to leave each sample with similar sequencing depth per cell. The total cell number was 22,700 with an average of 5675 ± 190 SEM cells per sample used for analysis (Dataset S1).

*Single cell RNA-sequencing clustering and differential expression (DE) analysis*

Unbiased cell type clustering was performed in the combined sample (wt-R-men, wt-R-par, Bcl6KO-R-men, Bcl6KO-R-par). Downstream analysis was performed with the R-package *Seurat* v3.1.1 (9) using R v3.6.1 as previously described (10). Briefly, low-quality cells and some cell doublets were removed by filtering cells with few genes (<500), high number of genes (>4500-5300) or high mitochondrial percentages (>4.5%). A further doublet depletion was done by R package *DoubletDecon* v1.1.4 (11) with default setting. After QC and doublet removal, the total remaining cell number used for further analysis was 16,068 with an average of 4,017 ± 132 SEM cells per sample (Dataset S1). Data were normalized using SCTransform (12). Data were regressed to cell cycle phase score with SCTransform. We used Principal component analysis

(PCA) for primary dimensionality reduction to identify the number of principal components for further analysis, and we performed an elbow plot.
PCA results were used for Uniform Manifold Approximation and Projection (UMAP). Clusters were identified by the “FindNeighbors” and “FindClusters” functions in Seurat. To better annotate the clusters, we queried differentially expressed (DE) genes in a literature search and plotted them in feature plots.
No cell clusters were removed. DE genes were identified by the “FindMarker” function in Seurat. DE genes were visualized in volcano plots with the R package *EnhancedVolcano* (13). DE gene lists include all cell clusters consisting of at least 10 cells used for comparison. Positive avg_logFC values describe a higher gene expression in the first mentioned of the two compared groups. DotPlots and FeaturePlots were created using the internal visualization functions of *Seurat*.

*Single cell TCR Repertoire sequencing from 3’ single cell cDNA libraries (Circularization scTCR-seq)*
The method “Circularization scTCR-seq” was recently developed by our group (16) and allowed the reconstruction of single cell antigen receptor information in cDNA generated by microfluidics-based 3’ barcoding scRNA-seq. This was achieved by shortening the constant region of antigen receptors during enrichment, while maintaining cell barcode and UMI information attached to the 3' end of the cDNA molecules. The sequence of the variable (VDJ) region of TCRs cannot be identified from microfluidics-based 3’ scRNA-seq with other approaches by short read sequencers such as Illumina’s platform, as the VDJ region is located near the 5’ end of the transcript (14) with constant region between VDJ region and 3’ cell barcode. The length of the constant (C) region reaches up to 1475 bp (15) and thus exceeds the maximum insert length (~700 bp) of short read sequencers (Fig. S3E), therefore no library containing both 3’ barcode and VDJ region sequence can be made by other approaches. Our new method allowed shortening the constant region of antigen receptors during enrichment, while maintaining their cell barcode and UMI information attached to the 3' of the cDNA molecules. In summary, the method used self-circulating the cDNA library to ligate the 3’ cell barcode with the 5’ end of the same molecule. To achieve this, the VDJ region was enriched together with the cell barcode, then self-circulated again and re-linearized to leave read1 at the 5’ end of the enriched fragments. Each step maintains the VDJ region together with the cell barcode and UMI in the same molecule (Fig S3E; details below).
First methods for microfluidics-based scRNA-seq were based on 3’-capturing (17, 18) and the ability to reconstruct antigen receptor sequences was achieved later by 5’-capturing (19). We here thus introduced an alternative approach (Fig. S3E). We see advantages of this approach, because it can reconstruct antigen receptor sequences from ‘older’ existing 3’ libraries, and it is theoretically compatible with RNA-capture in spatial transcriptomics.
Circularization scTCR-seq was performed as previously described (16). In detail, Primer *Poly A* was used as a 5’ race primer and two TCR reverse primer pools were designed according to the constant region sequence of the murine TCR. All primers were synthesized by Eurofins Genomics; the primer names, sequences and concentrations are listed in Dataset S23. For circularization, 25 ng of cDNA generated from the Chromium Single Cell 3' GEM Kit v3 (10x Genomics) were end-phosphated with the T4 Polynucleotide Kinase (New England Biolabs), and purified by 0.6x Ampure XP beads (Beckman Coulter). 1,000 units of T4 DNA Ligase (New England Biolabs) were added to self-circularize the phosphated cDNA in 25 µl total volume at 16°C for 16 hours. Subsequently, 0.7x Ampure XP beads were used for cDNA purification. Remaining linear DNA was digested by 0.9 units/µl RecJf and 0.1 units/µl Lambda Exonuclease (both from New England Biolabs). Circularized cDNA libraries were purified by 0.7x Ampure XP beads. A 5’ race nested PCR enrichment was performed to enrich the T cell receptor (TCR) variable region. Firstly, with 25 µl Kapa hotstart amplification mix (KAPA Biosystems), 10 µl primer *polyA* and 5 µl primer *TCR rev*

*pool_out* (Dataset S23); secondly with 25 µl Kapa hotstart amplification mix, 10 µl primer *polyA* and 5 µl primer *TCR rev pool_in* (Dataset S23). Because Primer Melting Temperatures are very different between primer Poly A and TCR rev primers, a 4 steps PCR (including 2 steps of annealing with different temperature, see Dataset S23) was used in both PCR steps. 0.5x - 0.8 x Ampure XP beads were used for subsequent size selection. Then, 25 ng of the nested PCR product were phosphated, circulated and linear digested again as above. A PCR with primers *read1* and *TSO* (Dataset S23) was used to re-linearize the circulated library (Fig. S3E). PCR products were purified by 0.5x - 0.8 x Ampure XP beads (Beckman Coulter) and libraries were prepared using the Chromium Single Cell 3' Library Kit v3 (10x Genomics). Sequencing was carried out commercially on an Illumina Novaseq with 150-8-8-150 read setup. Details regarding sequencing depth and cell recovery are provided in Dataset S1. A patent application covering the method for reconstructing TCR information from 3' libraries has been applied under the filing number LU101949.

The single cell TCR library has similar structures as the 10x Genomics 5' VDJ kit on read1 data but contains the reverse-complement sequence on read2 data. In order to use the cellranger VDJ pipeline (10x Genomics) to process our data, a reverse-complement modification of read2 data was done by using the SeqKit v0.11.0 (20). Because of the cell barcodes white lists difference between the 10x 3' v3 kit and the 10x 5' VDJ kit, we also replaced the cell barcodes white list of the 5' VDJ kit with the cell barcodes white list of 10x 3' v3 kit: In the folder of "/cellranger-3.1.0/cellranger-cs/3.1.0/lib/python/cellranger/barcodes/", we unzipped the file "3M-february-2018.txt.gz", renamed it as "737K-august-2016.txt" and replaced the same name file in the same folder. Processing of modified sequencing data was performed with the modified *cellranger VDJ* pipeline v3.1.0 (10X Genomics) according to the manufacturer's instructions with default settings.

In order to filter out possible mismatched cell barcodes during circularization, we introduced two filters that combined both scRNA-seq data and circularization scTCR-seq data to define possible 2D2 mouse derived T cells and confident 2D2 mouse derived T cells: 1) possible 2D2 mouse derived T cells using the following criteria: the cells contain any of CDR3 of 2D2 mouse T cell clonotype (TRA: CAVRSYNQGKLIF, TRB: CASSLDPGANTEVFF) in circularized scTCR-seq data and have at least 2 counts of total UMI of *Trac*, *Trbc1* and *Trbc2* transcripts in scRNAseq data. 2) confident 2D2 mouse derived T cells using the following criteria: the cells contain only CDR3 of 2D2 mouse T cell clonotype (TRA:CAVRSYNQGKLIF, TRB: CASSLDPGANTEVFF) in circularized scTCR-seq data and the ratios of their sum UMI count of *Trac*, *Trbc1* and *Trbc2* transcripts in the total RNA UMI counts are above 0.0025 in the scRNAseq data. We named confident 2D2-derived T cells as "2D2" cells and we named cells which do not match the 2D2 sequence as "non-2D2", and we named possible 2D2-derived T cells which are not confident 2D2 mouse derived T cells as "uncertain" (Dataset S1). In our scRNA-seq dataset, the known 2D2$^{tg}$ TCR α/β-sequence (2, 21) was identified in 30% of all α TCR chains and in 36% of all β TCR chains within the CD4$^+$ T cell clusters, respectively (Dataset S7). Single cell transcriptomes were classified as 2D2 when they expressed one or both chains of the 2D2$^{tg}$ TCR and expressed the *Trac/Trbc* mRNA at sufficient threshold.

*Bulk RNA-seq of sorted Vβ11$^+$ CD4$^+$ T cells*

Bulk RNA-seq was performed from flow sorted Vβ11$^+$CD4$^+$ T cells. These cells were either sorted from 1) *in vitro* differentiated Th17 cells immediately prior to intravenous injection for the induction of adoptive transfer (AT-) EAE, or 2) from leukocytes isolated *ex vivo* from AT-EAE recipient mice at peak of disease. Cells were sorted directly into 1.5 ml reaction tubes containing 100 µl RNA Lysis Buffer (Zymo Research). After sorting, tubes were vortexed, briefly centrifuged and stored at −80 °C until RNA isolation.

Samples for bulk RNA-seq were prepared using a modified version of the SmartSeq2 protocol (23). Briefly, total unquantified purified RNA using Quick-RNA Microprep Kit (Zymo Research) was used

as input. Reaction volumes were scaled up and the number of PCR cycles during cDNA amplification was adjusted accounting for the higher number of input cells compared to the original protocol (23). Library Preparation was done by the Next Ultra II FS DNA Library Prep Kit (New England Biolabs) using 1–3 ng of cDNA as input following the manufacturer's instructions. The rest of cDNA was kept for qPCR (see below). Sequencing was carried out on a NextSeq500 using the High-Out 75 cycle kit (Illumina) with 0-8-8-75 set up. Average read depth was 15.19 ± 0.65 SEM M reads per sample (Dataset S1).

*Bulk RNA expression quantification*

RNA-seq reads were trimmed by Trimmomatic v0.39 (24) and aligned to the RefSeq Mus musculus transcriptome (GRCm38) using HISAT2 (25). The resulting transcriptome alignments were sorted by SAMtools (26) and processed using the RNA-Seq by HTSeq (27) to estimate expected counts over RefSeq transcripts.

*Bulk RNA-seq data analysis*

Counted files were normalized and analyzed by R language package DESeq2 v1.28.1 (28)**.** Genes with expression count below 5 in all samples were filtered out. Differential Expression (DE) genes were calculated by DESeq2 v 1.28.1 with Wald test. The DE genes were visualized in venn diagrams and volcano plots with the R packages *VennDiagram* and *EnhancedVolcano* (13).

*Semi-quantitative (q)PCR*

$V\beta11^{+}CD4^{+}$ T cells were sorted as described. Amplified cDNA was generated using a modified version of the SmartSeq2 protocol (23) during the Bulk RNA-seq process (see above). The following material was used according to the manufacturer's protocol: Mastermix: Maxima Probe/ROX qPCR MM (2x) (Thermo Fisher), housekeeping gene *Gapdh* (Mm99999915_g1, VIC-MGB_PL labelled, TaqMan); tested TaqMan gene expression assays (FAM-MGB labelled): *Bcl6* (Mm00477633_m1), *Lta* (Mm00440228_gH), *Ltb* (Mm00434774_g1), *Il17a* (Mm00439618_m1).

*Collection of Cerebrospinal fluid and proteomics of chemokines and immunoglobulin isotypes*

Cerebrospinal fluid (CSF) was collected from mice as described (29). Mice were anesthetized at peak of EAE with intraperitoneal Ketamine / Xylazine. After removal of the hair and covering any pressure points of the skull with 2% xylocaine gel, the head of the mice was mounted in a stereotaxic apparatus (ASI Instruments) via ear bars (29). Under a dissecting binocular microscope, the skin and muscles were bluntly separated to expose the cisterna magna. The cisterna magna was exposed as a glistening and triangular shape (30, 31). Using the micromanipulators, the cisterna magna was punctured with a 30G blunt end Hamilton syringe and CSF was collected by pulling the piston back carefully. On average 15.92 µl +/- 1.58 SEM were collected from one mouse (Dataset S20). Samples were discarded if visibly red which indicated blood contamination. Mice were sacrificed afterwards.

The collected CSF was briefly centrifuged at 4°C, the supernatant was collected in low protein binding tubes, stored frozen at -80 °C until further processing. Detection of cytokines and chemokines was performed using the Bio-Plex Pro mouse chemokine panel 31-plex (Bio-Rad Laboratories, Hercules, CA) and analyzed by the Luminex FLEXMAP 3D platform as previously reported (32). Concentrations of CSF analytes were transformed logarithmically for graphing and statistical analysis purposes. Curve fitting was performed using Milliplex Analyst 5.0 software (VigeneTech.com).

Immunoglobulin (Ig) isotypes in CSF were evaluated using the ThermoFisher (Invitrogen) Antibody Isotyping 7-Plex Mouse ProcartaPlex™ Panel according to manufacturer's instructions. Briefly, CSF was diluted 1:75 with a universal assay buffer provided in the kit. Together with premixed

washed capture beads, 25 µl of the diluted sample was incubated for 1 hour at RT under continuous shaking (600 rpm). After washing steps on a magnet, the plate was incubated with isotyping detection antibody mix for 30 min at room temperature (600 rpm) and subsequently washed with a magnet. Read buffer was added and the plate was run on the Luminex® FLEXMAP 3D® detection instrument operated with xPONENT Software V4.2 (Luminex Corp., Austin, TX). Fifty beads per region for each bead were analyzed for mean fluorescence intensity (MFI) and compared to a 7-point standard curve. A 5-parameter curve fit algorithm was applied to the data using Belysa version 1.1.0 software (Merck EMD Millipore, Billerica, MA) to calculate the concentration of each analyte.

*Immunofluorescence stainings (IF)*

We used two different approaches for immunofluorescence stainings (IF) and histological analysis: 1) IF of whole spine cross-sections, and 2) frozen IF. The *first* approach was optimized to maintain the anatomy of whole spine cross-sections including intact meninges and to reduce the susceptibility of the tissue for changing its size during processing through protection by spinal bones. This approach was therefore suitable for quantification and localization in semi-quantitative heatmaps. The *second* approach was optimized for visualizing specific cell agglomerates at higher magnification and at improved feasibility of multi-color IF staining and optimized morphology. This was based on cryo sections which improve tissue conservation and multi-marker stainings.

*Whole-spine cross-section IF*

At peak of adoptive transfer EAE, mice were sacrificed for whole-spine histology as previously described (33, 34). Mice were perfused intracardially with PBS, followed by perfusion with 4% PFA. Spinal cord (SC) was dissected together with the surrounding bone. The tissue was fixed overnight in 4% PFA and then decalcified for seven days in 0.3 M EDTA solution. After 2-3 days the EDTA solution was changed once. The tissue was then cryoprotected with a 30% sucrose solution for at least two days. Cross-sections of the SC (10-µm thickness) were cut at the cervical, thoracic and lumbar level with a cryostat (Cryostar NX50) at -23 °C. After tissue blocking, the following primary antibodies were used for staining: hamster anti-mouse CD3 (clone 500A2, BD Bioscience, 1:30), rat anti-mouse FITC TCR Vβ11 (clone KT11, BioLegend, 1:50), rat anti-mouse B220 (clone RA3-6B2, Invitrogen, 1:200) and rat anti-mouse F4/80 (clone CI:A3-1, Serotec, 1:500). B220 staining was done with biotin-conjugated goat anti-rat IgG (Abcam, 1:200). F4/80 staining was enhanced using biotin-conjugated rabbit anti-rat IgG (Vector Labs, 1:200), streptavidin-horseradish peroxidase (Biolegend, 1:100) and tyramide (AdipoGen, 1:100 in elution buffer). For visualization the following fluorescent secondary antibodies were used: goat anti-rat IgG AF488 (ThermoFisher, 1:50), goat anti-hamster IgG AF594 (ThermoFisher, 1:50), streptavidin-conjugated AF488 (ThermoFisher, 1:100), streptavidin-conjugated AF594 (ThermoFisher, 1:100) and donkey anti-rabbit IgG AF594 (Life, 1:50). All antibodies were diluted in blocking reagent (Roche). Nuclei were stained by 4′,6-diamidino-2-phenylindole (DAPI) (included in used mounting medium Fluoromount-G with DAPI from Invitrogen). For intracellular Ki67 (rabbit anti-mouse, #ab15580, Abcam, 1:50) staining, cross-sections were permeabilized with 0.1% Triton before antibody staining. Ki67 staining was combined with labelled rat anti-mouse B220-AF488 (clone RA3-6B2, BD, dilution 1:100) and was otherwise done as described above.

We aimed to quantify infiltration by different cell types ($B220^+$, $F4/80^+$, $CD3^+$ and $V\beta11^+$ cells) at the cervical, thoracic and lumbar levels of the SC. To measure the whole compartment area (meninges & parenchyma), all stained sections were photographed (10x magnification) and the pictures were merged using BZ-Analyzer II (Keyence) to create overview pictures. The meninges were identified by their morphological structure between bone and parenchyma. The polygon and measurement functions of ImageJ were used to manually measure the compartment area from the overview pictures. The infiltrated area of $B220^+$ and $F4/80^+$ cells was measured in the same way and the

percentage of infiltrated area was determined by calculating the ratio between the total area of the compartment (meninges & parenchyma) and the infiltrated area of $B220^+$ and $F4/80^+$ cells contained in the compartment. The absolute number of $CD3^+$ and $V\beta11^+$ cells was counted manually in the compartments (meninges & parenchyma) on cervical, thoracic and lumbar level on the fluorescence microscope Nikon Eclipse 80i (40x magnification). To determine the absolute cell count of $Ki67^+B220^+$ cells, images of stained sections on lumbar level were taken with an apotome (Zeiss) in 20x magnification and cells were counted manually. The density of the infiltrated $CD3^+$, $V\beta11^+$ and $Ki67^+B220^+$ cells in the compartments [cells/$mm^2$] was determined by dividing the counted cells in each compartment by the area of that compartment.
Heatmaps were generated to map the localization of the different cell types. The heatmaps represent a schematic representation of the SC. Afterwards, heatmaps of the individual test mice were overlaid. The opacity of the infiltrates of the individual animals was calculated using the formula (100% / n) x 4. The digital editing was done with Adobe Illustrator CS6.

*Frozen IF*
At the peak of AT-EAE, mice were sacrificed, and spinal cord parenchyma enveloped in meninges was carefully isolated (without destroying the connected meningeal tissue). The tissue was directly frozen in Tissue-Tek O.C.T.™ compound (Sakura Finetek Europe) and stored at -80 °C until cutting. 8 µm longitudinal sections were cut at -20 °C using a cryotome (Microm International GmbH). Staining was performed as previously described (35, 36). Briefly, tissue was fixed in -20°C methanol for 10 minutes before the staining procedure and blocked in 1% BSA in PBS. Primary antibodies used for staining were rat anti-mouse B220-FITC or -AF488 (clone RA3-6B2, BD, dilution 1:100), rat anti-mouse B220 (unlabelled, clone RA3-6B2, eBiosciences, 1:50), rat anti-mouse TCR Vβ11-FITC or -APC (clone KT11, BioLegend, 1:100), rat anti-mouse CD4-APC (clone L3T4, eBioscience, 1:100), rat anti-mouse CD45.2 (clone 30G12, conditioned Medium, (37), undiluted), rabbit anti-mouse Laminin-111 'pan laminin' (38), Serum, 1:500), goat anti-mouse CXCL13 (R&D Systems, 1:50), rat anti-mouse ER-TR7 (clone ER-TR7, Dianova, 1:100). As secondary antibodies, donkey anti-rat IgG AF555 (1:3000), donkey anti-rat IgG AF647 (1:1000), donkey anti-rabbit IgG AF647 (1:1000), donkey anti-goat IgG AF594 (1:1000), donkey anti-rat IgG AF488 (1:1000), donkey anti-rabbit IgG AF594 (1:1000) were used. Nuclei were stained with DAPI and stained sections were mounted with Mowiol 488 (25% (w/v) in 1x PBS). Sections for high magnification were microscoped with Zeiss AxioImager (Software: Volocity 6.3 (PerkinElmer)). Overview pictures were acquired with a Zeiss LSM 700 confocal microscope using the ZEN grey/blue software (Zeiss).

*In vitro Th17 polarization and proliferation of $CD4^+$ T cells isolated from EAE mice*
$CD4^+$ T cells and $CD11c^+$ dendritic cells (DCs) were isolated from draining lymph nodes and spleen on day 10 after immunization with $MOG_{35-55}$ using magnetic beads (Miltenyi Biotec, anti-mouse CD4 (clone: L3T4) MicroBeads and anti-mouse CD11c UltraPure MicroBeads). $CD4^+$ T cells and $CD11c^+$ DCs were co-cultured in a 5:1 ratio in the presence of $MOG_{35-55}$ (20 µg/ml) on a round-bottom 96-well plate coated with anti-CD3 (0.5 µg/ml). For proliferation assays, $CD4^+$ T cells were additionally stained with CellTrace™ Violet (Thermofisher) according to manufacturer's instructions, and T cell proliferation was analyzed by flow cytometry. For Th17 polarization, TGF-β1 (10 ng/ml), IL-6 (20 ng/ml) and anti-IFN-γ (10 µg/ml) was added to the culture for 4 days, and intracellular cytokines were analyzed by flow cytometry after 4h of restimulation with PMA/ionomycin.

*In vitro B cell proliferation*

MOG-specific $CD19^+$ B cells were isolated with MicroBeads (Miltenyi Biotec, anti-mouse CD19 MicroBeads) from the spleen and inguinal lymph nodes of a naïve TH mouse (synonymously $IgH^{MOG}$ mouse, (5); containing a MOG-specific B cell receptor) and labeled with cell proliferation dye Cell Trace Violet (Thermofisher) according to manufacturer's instructions. Labeled B cells were cocultured in a 2:1 ratio with *in vitro* differentiated Th17 cells from $2D2^{tg}$ mice with $MOG_{35-55}$ peptide (3 µg/ml). Th17 had been differentiated as in AT-EAE (see above). On day 3, B cell proliferation was analyzed by flow cytometry.

*Statistics*

Data are presented as box-and-whisker plots (Tukey method) combined with dot plots. The hinges of the box extend from the $25^{th}$ to $75^{th}$ percentiles (= interquartile range, IQR), the horizontal line inside the box indicates the median, and the whiskers extend to the most extreme values within the 1.5 IQR of the lower and upper quartile. Dots illustrate the individual values. Data were compared using two-tailed Student's *t*-test for unrelated samples. If the F-test of equality of variances was significant, the two-tailed Mann-Whitney U test was applied. $p\text{-value} < 0.05$ was considered significant. The correlation analysis for normally distributed data (checked by Shapiro-Wilk and Kolmogorov-Simnov) was carried out with the one-tailed Pearson test. Otherwise, the Spearman test was used. GraphPad Prism 5 was used for statistical analysis of quantifications of flow cytometry, immunohistochemistry, qPCR, and CSF proteomics data. Statistical analysis of sequencing data was done in R v3.6.1.

Figure S1

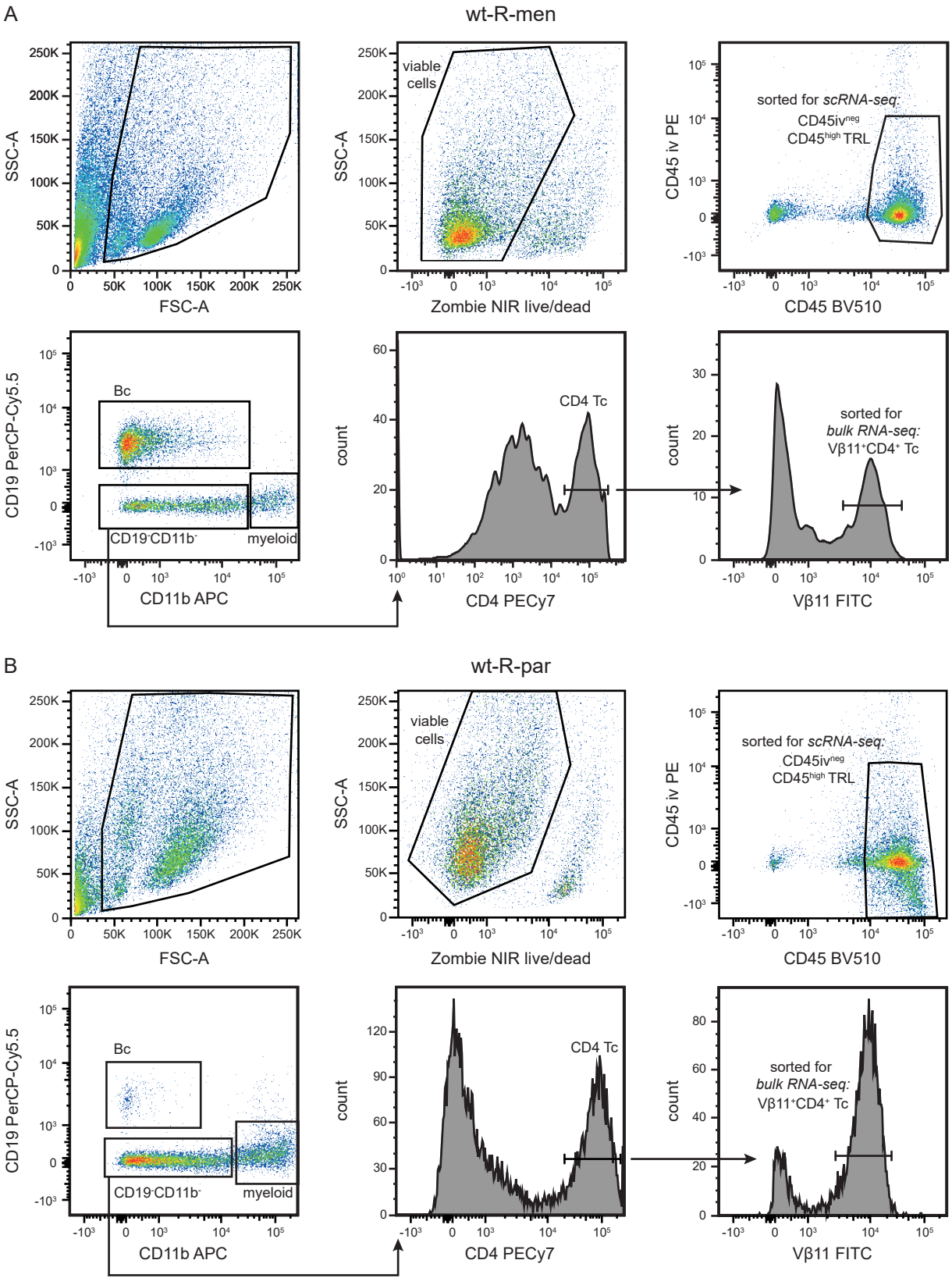
A
wt-R-men
SSC-A
FSC-A
viable cells
Zombie NIR live/dead
CD45 iv PE
CD45 BV510
sorted for scRNA-seq:
CD45iv^neg
CD45^high TRL
CD19 PerCP-Cy5.5
CD11b APC
Bc
CD19-CD11b-
myeloid
count
CD4 Tc
CD4 PECy7
sorted for
bulk RNA-seq:
Vβ11+CD4+ Tc
Vβ11 FITC
B
wt-R-par

***Figure S1****: Representative gating strategies of FACS and flow cytometry.*
(A) Representative gating of the indicated cell types in the meninges (men) and (B) the parenchyma (par) of the spinal cord of recipients of wild type 2D2$^{tg}$ Th17 donor cells (wt-R) to identify main lineages and to flow sort for CD45iv$^{neg}$ tissue-resident viable leukocytes (TRL) - either CD45$^{high}$ leukocytes for scRNA-seq or Vβ11$^{+}$ CD4$^{+}$ T cells (Tc) for bulk RNA-seq. Abbreviations: *scRNA-seq* single cell RNA sequencing, *bulk RNA-seq* bulk RNA sequencing.

Figure S2

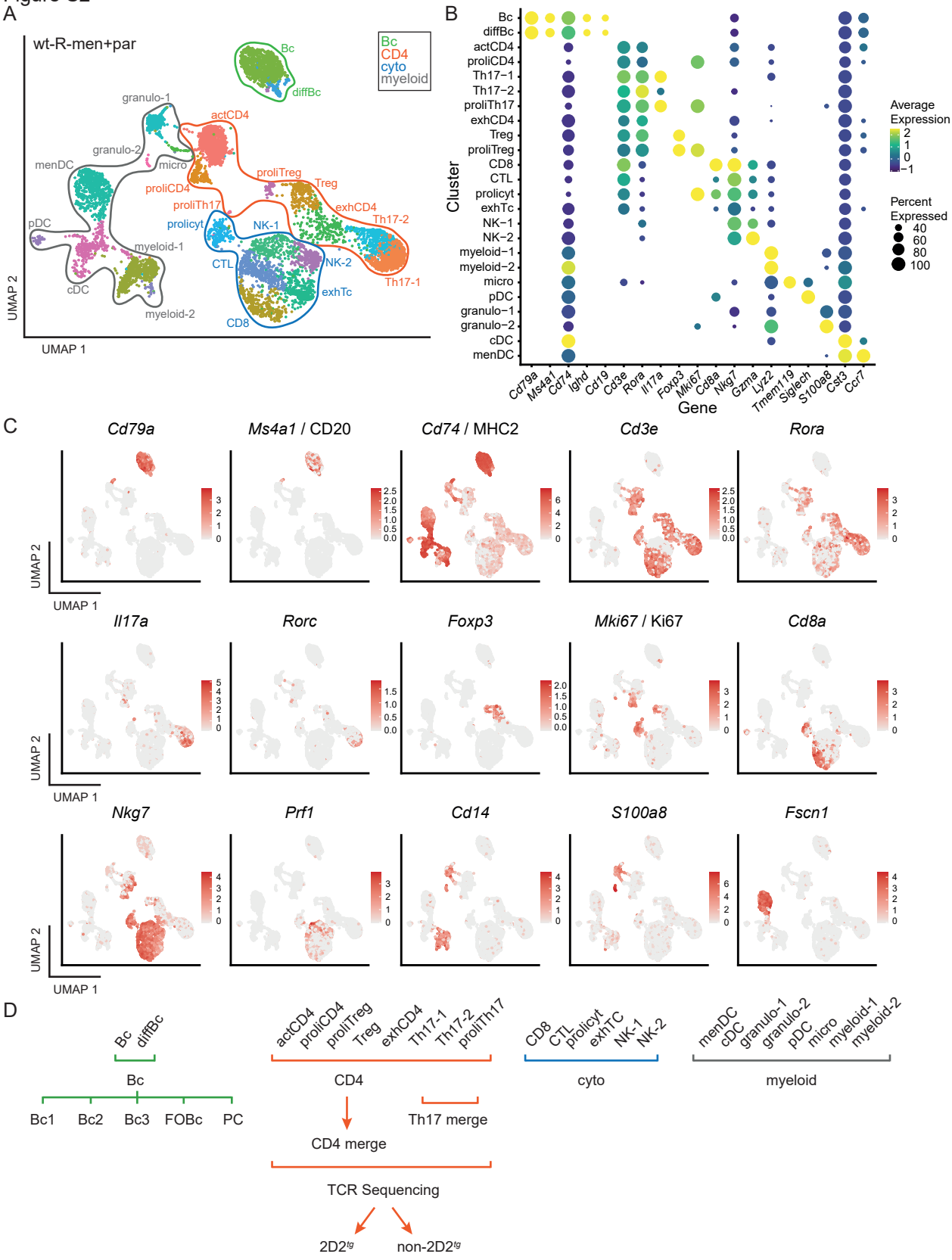
A
wt-R-men+par
Bc
CD4
cyto
myeloid
Bc
diffBc
granulo-1
actCD4
granulo-2
menDC
micro
proliTreg
Treg
proliCD4
proliTh17
exhCD4
Th17-2
pDC
prolicyt
NK-1
myeloid-1
CTL
NK-2
Th17-1
cDC
exhTc
myeloid-2
CD8
UMAP 2
UMAP 1
B
Cluster
Bc
diffBc
actCD4
proliCD4
Th17−1
Th17−2
proliTh17
exhCD4
Treg
proliTreg
CD8
CTL
prolicyt
exhTc
NK−1
NK−2
myeloid−1
myeloid−2
micro
pDC
granulo−1
granulo−2
cDC
menDC
Cd79a
Ms4a1
Cd74
Igkd
Cd19
Cd3e
Rora
Il17a
Foxp3
Mki67
Cd8a
Nkg7
Gzma
Lyz2
Tmem119
Siglech
S100a8
Cst3
Ccr7
Gene
Average Expression
2
1
0
−1
Percent Expressed
40
60
80
100
C
Cd79a
Ms4a1 / CD20
Cd74 / MHC2
Cd3e
Rora
Il17a
Rorc
Foxp3
Mki67 / Ki67
Cd8a
Nkg7
Prf1
Cd14
S100a8
Fscn1
UMAP 2
UMAP 1
D
Bc
diffBc
Bc
Bc1
Bc2
Bc3
FOBc
PC
actCD4
proliCD4
proliTreg
Treg
exhCD4
Th17-1
Th17-2
proliTh17
CD4
Th17 merge
CD4 merge
CD8
CTL
prolicyt
exhTC
NK-1
NK-2
cyto
menDC
cDC
granulo-1
granulo-2
pDC
micro
myeloid-1
myeloid-2
myeloid
TCR Sequencing
2D2tg
non-2D2tg

***Figure S2****: Combined cell cluster characterization and annotation.*
(A) CD45iv$^{neg}$CD45$^{high}$ tissue-resident leukocytes (TRL) were flow sorted from the spinal cord meninges (men) and parenchyma (par) of recipients of wild type (wt) 2D2$^{tg}$ Th17 donor cells (wt-R) and processed by single cell RNA-sequencing (scRNA-seq). Single cell transcriptomes from two combined samples (wt-R-men: 4,068 cells, wt-R-par: 4,071 cells) are depicted in a Uniform Manifold Approximation and Projection (UMAP) plot. Clusters are classified and outlined as B cells (Bc; green), CD4$^+$ T cells (CD4; orange), CD8$^+$ T and natural killer cells (cyto; blue), and myeloid cells (grey). Description of all Bc and CD4 clusters as in Fig. 1B (Results). Cytotoxic and myeloid clusters were defined as followed: Six clusters were assigned to cytotoxic cell types (cyto) and represented CD8 T cells (*Cd3e*, *Cd8a*, *Ccl5*, *Nkg7*), cytotoxic T lymphocytes (CTL; *Cd3e*, *Nkg7*) and two types of natural killer (NK) cells (*Nkg7*, *Cd3e$^{neg}$*, *Prf1*, *Gzma*). Eight myeloid lineage clusters represented plasmacytoid dendritic cells (pDC; *Siglech*), two clusters of granulocytes (granulo-1/granulo-2; *S100a8*, *Lcn2*), classical dendritic cells (cDC; *Clec9a*, *Cst3*, *Cd74*/MHC class II chain) and meningeal dendritic cells (menDC; *Fscn1*, *Ccr7*, *Cst3*). Others resembled microglia (micro; *Hexb*, *Tmem119*) and two further myeloid clusters (myeloid-1/-2; *Lyz2*, *Cd14*, *Fcgr3*/CD16) as described (39, 40). (B) Dotplot of selected marker genes for main leukocyte lineages in the combined dataset as in A. (C) Feature plots of selected marker genes for main leukocyte lineages. (D) Scheme illustrating the clustering and cell classification approach. The initial 24 cell clusters were classified into 4 cell types and B cells were further sub-clustered. All CD4 clusters and all Th17 clusters, respectively, were merged for deeper transcriptomic analysis depicted in Fig. S3A-B. All clusters identified as CD4$^+$ T cells were subset into cells expressing the 2D2$^{tg}$ T cell receptor (TCR) or expressing other non-2D2$^{tg}$ TCRs.

Abbreviations: *Bc* B cells, *diffBc* differentiated B cells, *CD4* CD4$^+$ T cells, *act* activated, *Th17* Th17 cells, *Treg* regulatory T cells, *proli* proliferating, *exh* exhausted, *CD8* CD8$^+$ T cells, *CTL* cytotoxic T lymphocytes, *NK* natural killer cells, *prolicyt* proliferating cytotoxic T lymphocytes, *granulo* granulocytes, *micro* microglia, *DC* dendritic cells, *menDC* meningeal DC, *pDC* plasmacytoid DC, *cDC* classical DC, *myeloid* myeloid cells.

Figure S3

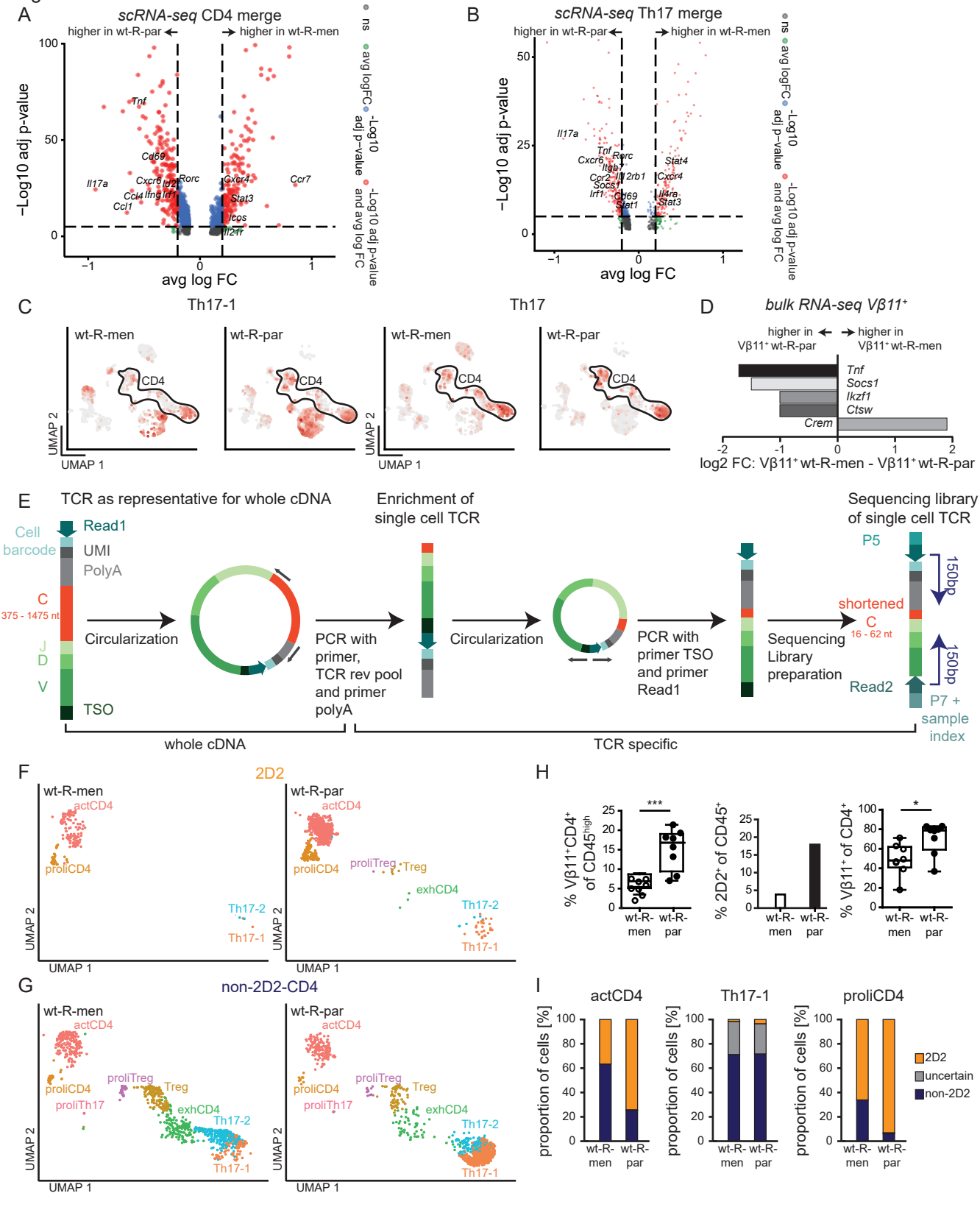
A
scRNA-seq CD4 merge
higher in wt-R-par
higher in wt-R-men
−Log10 adj p-value
avg log FC
ns
avg logFC
−Log10 adj p-value
−Log10 adj p-value and avg log FC
Tnf
Cd69
Il17a
Cxcr6
Il2
Rorc
Cxcr4
Ccr7
Ccl4
Ifng
Irf1
Ccl1
Stat3
Icos
Il2rb
B
scRNA-seq Th17 merge
higher in wt-R-par
higher in wt-R-men
−Log10 adj p-value
avg log FC
ns
avg logFC
−Log10 adj p-value
−Log10 adj p-value and avg log FC
Il17a
Tnf
Rorc
Cxcr6
Itgb1
Ccr2
Il2rb1
Socs1
Irf1
Cd69
Stat1
Stat4
Cxcr4
Il4ra
Stat3
C
Th17-1
Th17
wt-R-men
wt-R-par
CD4
UMAP 2
UMAP 1
D
bulk RNA-seq Vβ11+
higher in Vβ11+ wt-R-par
higher in Vβ11+ wt-R-men
Tnf
Socs1
Ikzf1
Ctsw
Crem
log2 FC: Vβ11+ wt-R-men - Vβ11+ wt-R-par
E
TCR as representative for whole cDNA
Enrichment of single cell TCR
Sequencing library of single cell TCR
Cell barcode
Read1
UMI
PolyA
C
375 - 1475 nt
J
D
V
TSO
Circularization
PCR with primer, TCR rev pool and primer polyA
Circularization
PCR with primer TSO and primer Read1
Sequencing Library preparation
P5
shortened C
16 - 62 nt
Read2
P7 + sample index
150bp
150bp
whole cDNA
TCR specific
F
2D2
wt-R-men
wt-R-par
actCD4
proliCD4
proliTreg
Treg
exhCD4
Th17-2
Th17-1
UMAP 2
UMAP 1
G
non-2D2-CD4
wt-R-men
wt-R-par
actCD4
proliCD4
proliTreg
Treg
proliTh17
exhCD4
Th17-2
Th17-1
UMAP 2
UMAP 1
H
% Vβ11+CD4+ of CD45high
% 2D2+ of CD45+
% Vβ11+ of CD4+
***
*
wt-R-men
wt-R-par
I
actCD4
Th17-1
proliCD4
proportion of cells [%]
2D2
uncertain
non-2D2
wt-R-men
wt-R-par

***Figure S3****: The meningeal vs. parenchymal microenvironment induces a site-specific CD4⁺ T cell phenotype in neuroinflammation.*

(A) Single cell transcriptomes of AT-EAE wt-R (Fig. 1B) and identified as $CD4^+$ T cells (actCD4, proliCD4, proliTreg, Treg, exhCD4, Th17-1, Th17-2, proliTh17) or as (B) Th17 cells (Th17-1, Th17-2, proliTh17) were combined, and genes differentially expressed (DE) between meninges (men) and parenchyma (par) (Dataset S3-4) were depicted as volcano plots. Genes beginning with 'Mt' and 'Rp' were removed. Thresholds for significant genes were set at average (avg) log Fold Change (FC) > 0.02 and -Log10 adjusted (adj) p-value < 1E-05. (C) Gene score plots of selected genes characteristic for Th17-1 (left) or Th17 cells (right) in men and par (Dataset S5). Black border line highlights $CD4^+$ T cells. (D) $V\beta11^+CD4^+CD45iv^{neg}CD45^{high}$ cells were sorted from men and par of the SC of a wt-R at peak AT-EAE (illustrated in Fig. 1A) and processed by bulk RNA-sequencing. Bar plots of genes DE in $V\beta11^+$ wt-R-men vs. $V\beta11^+$ wt-R-par (Dataset S6). (E) 'Circularization' protocol for obtaining antigen receptor information from 3' scRNA-seq (Suppl. Methods). The first circularization step is completed for the whole cDNA from scRNA-seq library, the second circularization step (after enrichment of single cell T cell receptor (TCR)) is TCR-specific. The result is a substantial shortening of the TCR constant region enabling sequencing of the TCR variable region. (F) UMAP plot with $CD4^+$ T cells expressing the $2D2^{tg}$ TCR in wt-R-men (left) and wt-R-par (right). (G) UMAP plot of $CD4^+$ T cells expressing any non-$2D2^{tg}$ TCR in wt-R-men (left) and wt-R-par (right). (H) Comparison of the proportion of 2D2 cells: $V\beta11^+CD4^+$ of $CD45^{high}$ tissue-resident leukocytes (TRL) in wt-R-men vs. wt-R-par quantified by flow cytometry (left), and $2D2^{tg}$ TCR expressing $CD4^+$ T cells determined by TCR sequencing related to all leukocytes ($CD45^{high}$), i.e. all cells included in the scRNA seq dataset (middle). Right: proportion of $V\beta11^+$ of viable $CD4^+$ (TRL) quantified by flow cytometry. TRL analyzed by flow cytometry or scRNA seq were isolated from SC meninges and parenchyma of wt-R (peak AT-EAE). (I) Stacked bar-plots of the proportion of $2D2^{tg}$ TCR and non-$2D2^{tg}$ TCR within selected CD4 clusters (with high proportion of $2D2^{tg}$ TCR expressing cells) in wt-R-men vs. wt-R-par. $CD4^+$ T cells were classified by single cell transcriptomes; $2D2^{tg}$ TCR cells by the expression of the known $2D2^{tg}$ TCR α/β-sequence and a sufficient expression of the *Trac/Trbc* mRNA.

Abbreviations: *AT-EAE* adoptive transfer experimental autoimmune encephalomyelitis, *wt-R* wild type recipient, *act* activated, *proli* proliferating, *exh* exhausted, *SC* spinal cord.

Figure S4

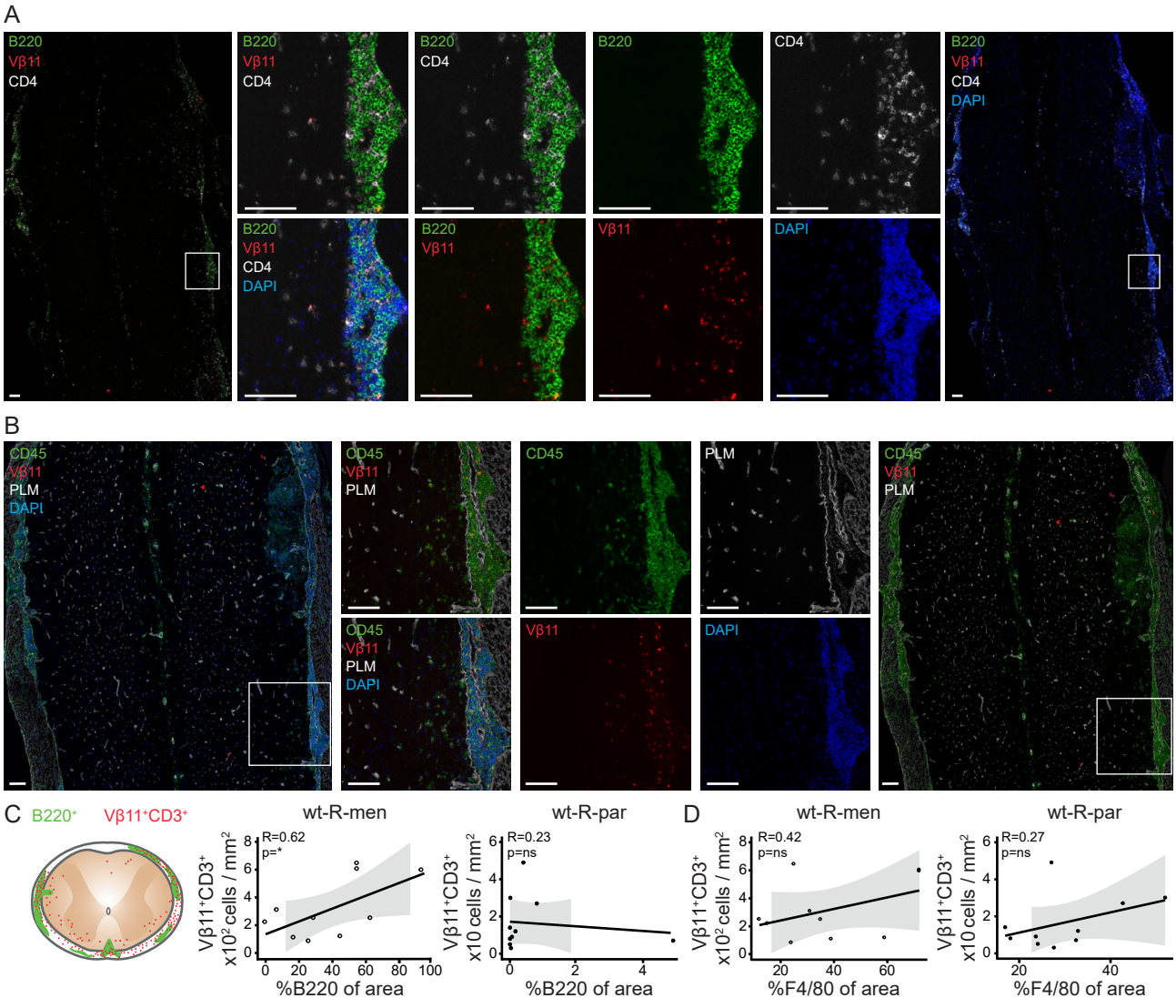
A
B220
Vβ11
CD4
DAPI
B
CD45
PLM
C
B220⁺
Vβ11⁺CD3⁺
wt-R-men
wt-R-par
Vβ11⁺CD3⁺ x10² cells / mm²
Vβ11⁺CD3⁺ x10 cells / mm²
R=0.62
p=*
R=0.23
p=ns
%B220 of area
D
R=0.42
p=ns
R=0.27
p=ns
%F4/80 of area

***Figure S4****: B cells and donor-derived CD4 T cells colocalize in spinal cord meninges of AT-EAE recipient mice.*

(A-B) Representative immunofluorescence staining of parallel freshly frozen SC longitudinal sections (Methods) of a AT-EAE recipient (wt-R) mouse at peak of disease stained for the indicated markers. Scale bars indicate 100 µm. Overview pictures on the left and right side include a magnification box indicating the exact location of the enlarged section shown in different color combinations. *PLM* pan laminin marker (Methods). This Suppl. Fig. is related to Fig. 1H. (C) Heatmap (left) represents the localization of $B220^+$ areas and $V\beta11^+CD3^+$ cells in a lumbar cross-section of one representative AT-EAE recipient (wt-R) mouse at peak of disease. Dot plots depicting correlations between $V\beta11^+$ and $B220^+$ cell densities in the meninges (men; middle) (top; r=0.62, $R^2$=0.38, p=0.03), however not in the parenchyma (par; right) of AT-EAE recipients (wt-R). (D) Dotplots depicting lacking correlations between $V\beta11^+$ and $F4/80^+$ cell densities in the men (left; r=0.42, $R^2$=0.18, p=0.12) and par (right; r=0.28, $R^2$=0.17, p=0.22) of wt-R. Straight line represents the linear regression line with its confidence interval in grey in C and D.

Abbreviations: *AT-EAE* adoptive transfer experimental autoimmune encephalomyelitis.

Figure S5

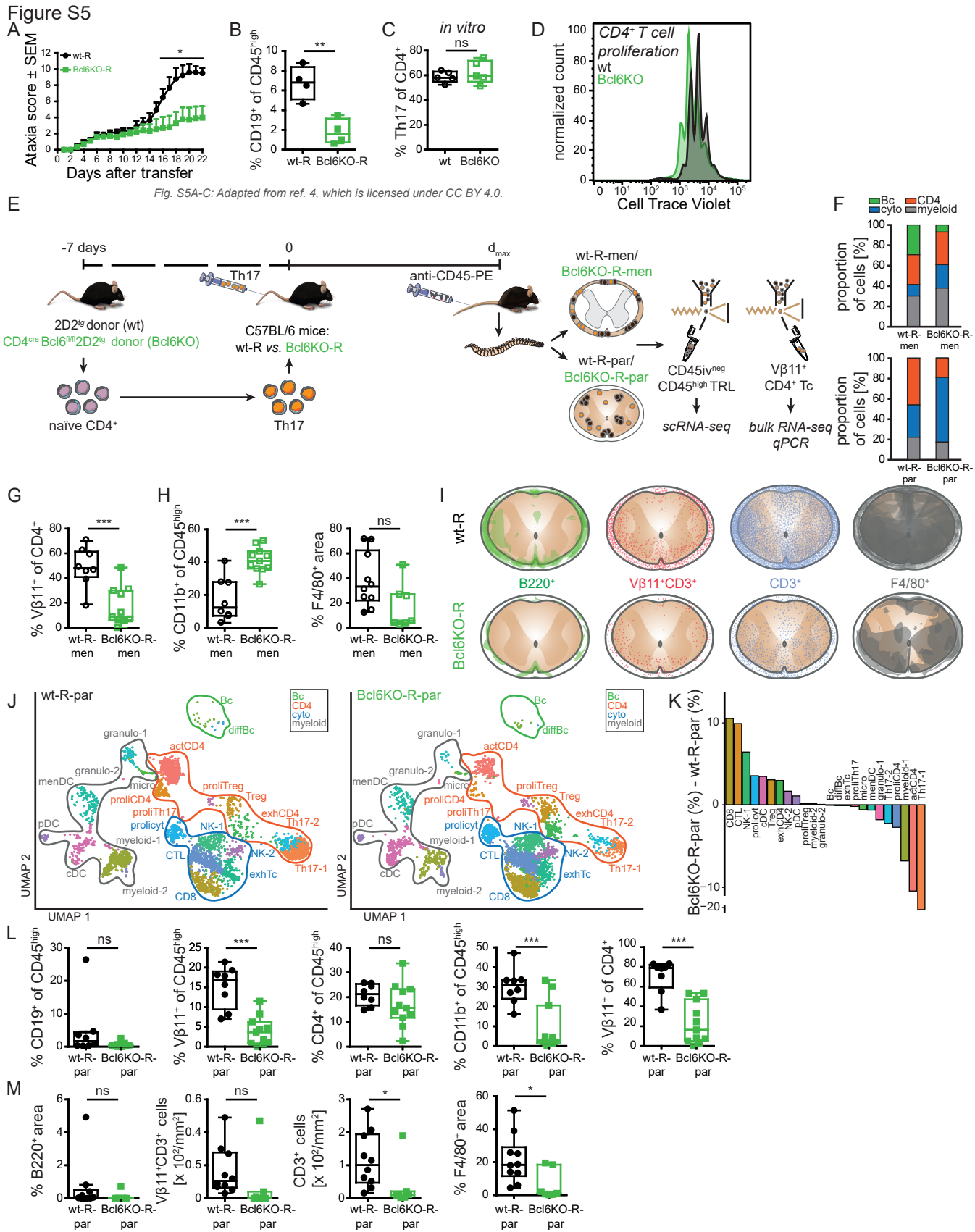
A
Ataxia score ± SEM
wt-R
Bcl6KO-R
Days after transfer
B
% CD19+ of CD45high
wt-R
Bcl6KO-R
C
in vitro
% Th17 of CD4+
ns
wt
Bcl6KO
D
CD4+ T cell proliferation
wt
Bcl6KO
normalized count
Cell Trace Violet
Fig. S5A-C: Adapted from ref. 4, which is licensed under CC BY 4.0.
E
-7 days
0
dmax
Th17
anti-CD45-PE
2D2tg donor (wt)
CD4cre Bcl6fl/fl2D2tg donor (Bcl6KO)
naïve CD4+
C57BL/6 mice:
wt-R vs. Bcl6KO-R
Th17
wt-R-men/
Bcl6KO-R-men
wt-R-par/
Bcl6KO-R-par
CD45ivneg
CD45high TRL
scRNA-seq
Vβ11+
CD4+ Tc
bulk RNA-seq
qPCR
F
Bc
cyto
CD4
myeloid
proportion of cells [%]
wt-R-men
Bcl6KO-R-men
wt-R-par
Bcl6KO-R-par
G
% Vβ11+ of CD4+
wt-R-men
Bcl6KO-R-men
H
% CD11b+ of CD45high
% F4/80+ area
I
wt-R
Bcl6KO-R
B220+
Vβ11+CD3+
CD3+
F4/80+
J
wt-R-par
Bcl6KO-R-par
Bc
CD4
cyto
myeloid
diffBc
granulo-1
granulo-2
menDC
micro
actCD4
proliCD4
proliTh17
prolicyt
proliTreg
Treg
exhCD4
Th17-2
NK-1
NK-2
CTL
exhTc
Th17-1
pDC
cDC
myeloid-1
myeloid-2
CD8
UMAP 1
UMAP 2
K
Bcl6KO-R-par (%) - wt-R-par (%)
CD8
CTL
NK-1
prolicyt
cDC
Treg
exhCD4
NK-2
pDC
proliTreg
myeloid-2
granulo-2
Bc
diffBc
exhTc
proliTh17
micro
menDC
granulo-1
Th17-2
proliCD4
myeloid-1
actCD4
Th17-1
L
% CD19+ of CD45high
% Vβ11+ of CD45high
% CD4+ of CD45high
% CD11b+ of CD45high
% Vβ11+ of CD4+
M
% B220+ area
Vβ11+CD3+ cells [x 10²/mm²]
CD3+ cells [x 10²/mm²]
% F4/80+ area

***Figure S5**: Histology confirms that Bcl6 differentially affects T cells and B cells in neuroinflammation.*

(A) Recipient (-R) mice of $2D2^{tg}$ (wild type (wt), black circles, n = 6) and $CD4^{Cre}Bcl6^{fl/fl}2D2^{tg}$ (Bcl6KO, green squares, n = 8) were monitored for signs of AT-EAE (scheme of experimental set-up described and depicted in Fig. S5E). One representative out of five independent experiments is shown. Adapted from (4) in accordance with the Creative Commons license "CC BY 4.0" (https://creativecommons.org/licenses/by/4.0/). (B) Proportion of $CD19^+$ $CD3^-$ B cells of $CD45^{high}$ leukocytes isolated from the brain and spinal cord (SC). Parenchymal and meningeal tissues were not separated here. Adapted from (4), which is licensed under CC BY 4.0. (C) *In vitro* differentiated Th17 cells from wild type (wt) $2D2^{tg}$ donors or from $CD4^{Cre}Bcl6^{fl/fl}2D2^{tg}$ (Bcl6KO) donors immediately before adoptive transfer (Fig. 1, Fig. S5E) were re-stimulated for 4 hours with PMA/ionomycin and stained for intracellular cytokines. Adapted from (4), which is licensed under CC BY 4.0. (D) Wt or $CD4^{Cre}Bcl6^{fl/fl}$ (Bcl6KO) mice were immunized with $MOG_{35-55}$ and after 10 days, $CD4^+$ T cells were isolated from iLN and spleen, labeled with Cell Trace Violet, and co-cultured for 4 days with $CD11c^+$ and $MOG_{35-55}$ (Methods). T cell proliferation was analyzed by flow cytometry. (E) Scheme illustrating the experimental approach: Naïve $CD44^{low}CD62L^{high}CD4^+$ T cells (violet) were sorted from $2D2^{tg}$ (wt) and $2D2^{tg}$ $CD4^{cre}$ $Bcl6^{fl/fl}$ (Bcl6KO) donor mice and differentiated *in vitro* into Th17 donor cells (orange) with TGF-β1/IL-6 followed by IL-23 (41). These were intravenously (iv) injected into C57BL/6 recipient (=R) mice (= wt-R / Bcl6KO-R) to induce adoptive transfer experimental autoimmune encephalomyelitis (AT-EAE; Methods). At maximum AT-EAE severity, phycoerythrin (PE) labelled anti-CD45 antibody (3 µg/mouse) was iv injected and leukocytes were separately extracted from the meninges (men; top) and parenchyma (par; bottom) of the SC. $CD45iv^{neg}CD45^{high}$ cells were defined as tissue-resident leukocytes (TRL) and flow sorted for single cell RNA-sequencing (scRNA-seq) and $V\beta11^+CD4^+CD45iv^{neg}$ T cells (Tc) were sorted for bulk RNA-seq and qPCR (Methods; sorting strategy shown in Fig. S1). (F) Stacked bar-plots of the proportions of cell types classified in Fig. 1B and Fig. 2D in wt-R-men and Bcl6KO-R-men (upper panels) and wt-R-par and Bcl6KO-R-par (bottom panels). (G) Proportion of $V\beta11^+$ cells of viable $CD4^+CD45iv^{neg}CD45^{high}$ TRL in the meninges of wt-R (black open circles) and Bcl6KO-R (green open squares) was quantified by flow cytometry. (H) Proportion of $CD11b^+$ cells of viable $CD45iv^{neg}CD45^{high}$ TRL in the meninges of wt-R and Bcl6KO-R was quantified by flow cytometry (left). Proportion of F4/80 infiltrated area in the meninges of wt-R and Bcl6KO-R (right) was quantified by IF (Methods). (I) Frozen PFA-fixed cross-sections of the SC inside the decalcified vertebrae were stained by immunofluorescence. The area occupied by $B220^+$ (left) and $F4/80^+$ cells (right) and the number of $V\beta11^+CD3^+$ and $CD3^+$ cells (middle) were quantified and localized manually (Methods). Heatmaps represent overlays of n = 10 wt-R mice (upper panels) and n = 7 Bcl6KO-R mice (bottom panels) of lumbar SC sections in every panel. (J) UMAP plot depicting single cell transcriptomes of TRL extracted from SC parenchyma (par) of wt-R (wt-R-par, 4,071 cells) and Bcl6KO-R (Bcl6KO-R-par, 4,279 cells). (K) Bi-directional bar-plots showing differences of cluster proportions in Bcl6KO-R-par vs. wt-R-par. Positive values indicate higher abundance in the Bcl6KO-R-par. (L) Proportions of the indicated cell types were quantified by flow cytometry of viable $CD4^+CD45iv^{neg}CD45^{high}$ TRL or of viable $CD45iv^{neg}CD45^{high}$ TRL in the parenchyma of wt-R (closed black circles) and Bcl6KO-R (closed green squares). Gating of flow cytometry analyses (G-H, L) as in Fig. 1E and Fig. S1. (M) Quantification of % area occupied by $B220^+$ (left) and $F4/80^+$ cells (right), or the density of $V\beta11^+CD3^+$ and $CD3^+$ cells (middle) in SC parenchyma of wt-R and Bcl6KO-R as in I. Each dot represents the mean of three SC sections per mouse. Median, 25th-to-75th percentiles, and 1.5-fold interquartile range indicated in G-H, L-M. Student's t-test was used for all normally distributed datasets, otherwise Mann-Whitney-U test was used (Methods). * $p < 0.05$, ** $p < 0.01$, *** $p < 0.001$, ns not significant.

Abbreviations: *AT-EAE* adoptive transfer experimental autoimmune encephalomyelitis.

Figure S6

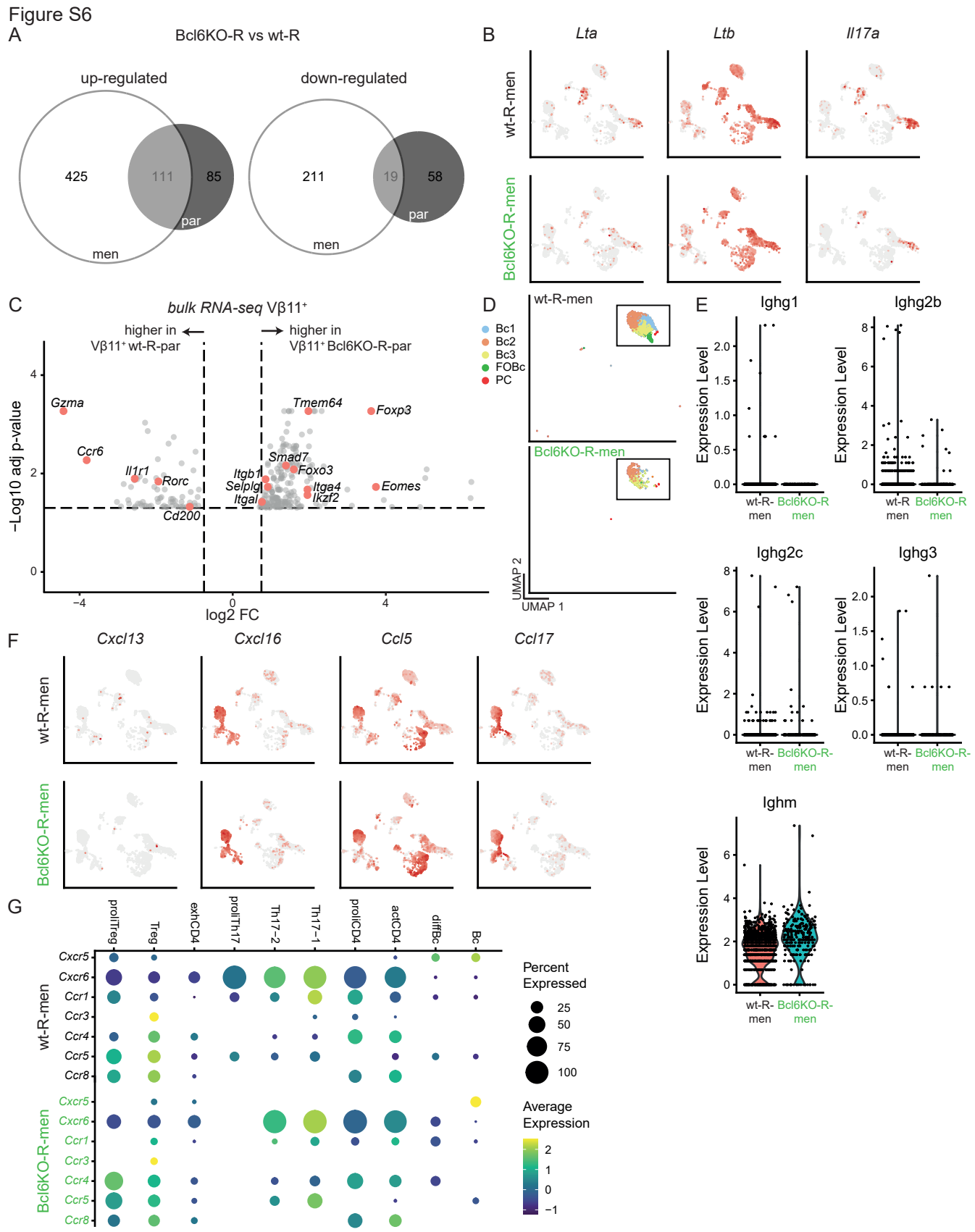
A
Bcl6KO-R vs wt-R
up-regulated
down-regulated
425
111
85
211
19
58
par
men
B
Lta
Ltb
Il17a
wt-R-men
Bcl6KO-R-men
C
bulk RNA-seq Vβ11+
higher in Vβ11+ wt-R-par
higher in Vβ11+ Bcl6KO-R-par
−Log10 adj p-value
log2 FC
Gzma
Ccr6
Il1r1
Rorc
Cd200
Tmem64
Foxp3
Smad7
Foxo3
Itgb1
Selplg
Itgal
Itga4
Ikzf2
Eomes
D
wt-R-men
Bcl6KO-R-men
Bc1
Bc2
Bc3
FOBc
PC
UMAP 2
UMAP 1
E
Ighg1
Ighg2b
Ighg2c
Ighg3
Ighm
Expression Level
wt-R-men
Bcl6KO-R-men
F
Cxcl13
Cxcl16
Ccl5
Ccl17
wt-R-men
Bcl6KO-R-men
G
proliTreg
Treg
exhCD4
proliTh17
Th17−2
Th17−1
proliCD4
actCD4
diffBc
Bc
Cxcr5
Cxcr6
Ccr1
Ccr3
Ccr4
Ccr5
Ccr8
wt-R-men
Bcl6KO-R-men
Percent Expressed
25
50
75
100
Average Expression
2
1
0
−1

***Figure S6**: Bcl6 in Th17 cells changes the cell communication in spinal cord meninges in neuroinflammation.*

(A) $V\beta11^{+}CD4^{+}CD45iv^{neg}CD45^{high}$ cells sorted from the meninges (men) or parenchyma (par) of the spinal cord (SC) of wild type (wt) and Bcl6KO recipients (-R) at peak AT-EAE were processed by bulk RNA-sequencing as in Fig. 2A (Fig. S5E), and meningeal- or parenchymal-specific differentially expressed (DE) genes between Bcl6KO-R and wt-R were calculated. Venn diagrams depict the number of up- (left) or downregulated (right) DE genes in Bcl6KO-R compared to wt-R (Dataset S15,16) in men (white circle), par (black circle) or in both men and par (grey circle). (B) Feature plots of selected genes in wt-R-men and Bcl6KO-R-men. (C) Volcano plot shows DE genes between Bcl6KO-R and wt-R in donor-derived cells sorted from the SC parenchyma (peak AT-EAE) and analyzed by bulk-RNA sequencing as described in A. Thresholds were set at -Log10 adjusted p value < 0.05 and log2FC > 0.75. (Dataset S15). (D) Single cell transcriptomes identified as B cells (Bc; *Bc* and *diffBc* cluster) were sub-clustered in wt-R-men (upper panel) and Bcl6KO-R-men (bottom panel). Plots represent zoom out of comparative Uniform Manifold Approximation and Projection (UMAP) plots shown in Fig. 3B. (E) Violin plots depict selected Igh gene expression level in merged Bc from wt-R-men vs. Bcl6KO-R-men analyzed by single cell RNA-seq. One dot represents one single cell. (F) Feature plots of selected chemokine markers in wt-R-men (upper plots) vs. Bcl6KO-R-men (bottom plots). (G) Dot plot with selected chemokine receptors that can bind to the chemokine markers depicted in Fig. S6F in clusters identified as B cells and CD4 T cells in Fig. 1B and Fig. 2D. Upper dotplot shows marker expression in wt-R-men, bottom plot in Bcl6KO-R-men.

Abbreviations: *log(2)FC* log(2) fold change, *Bc* B cells, *diffBc* differentiated B cells, *CD4* $CD4^{+}$ T cells, *act* activated, *proli* proliferating, *Th17* Th17 cells, *exh* exhausted, *Treg* regulatory T cells.

Figure S7

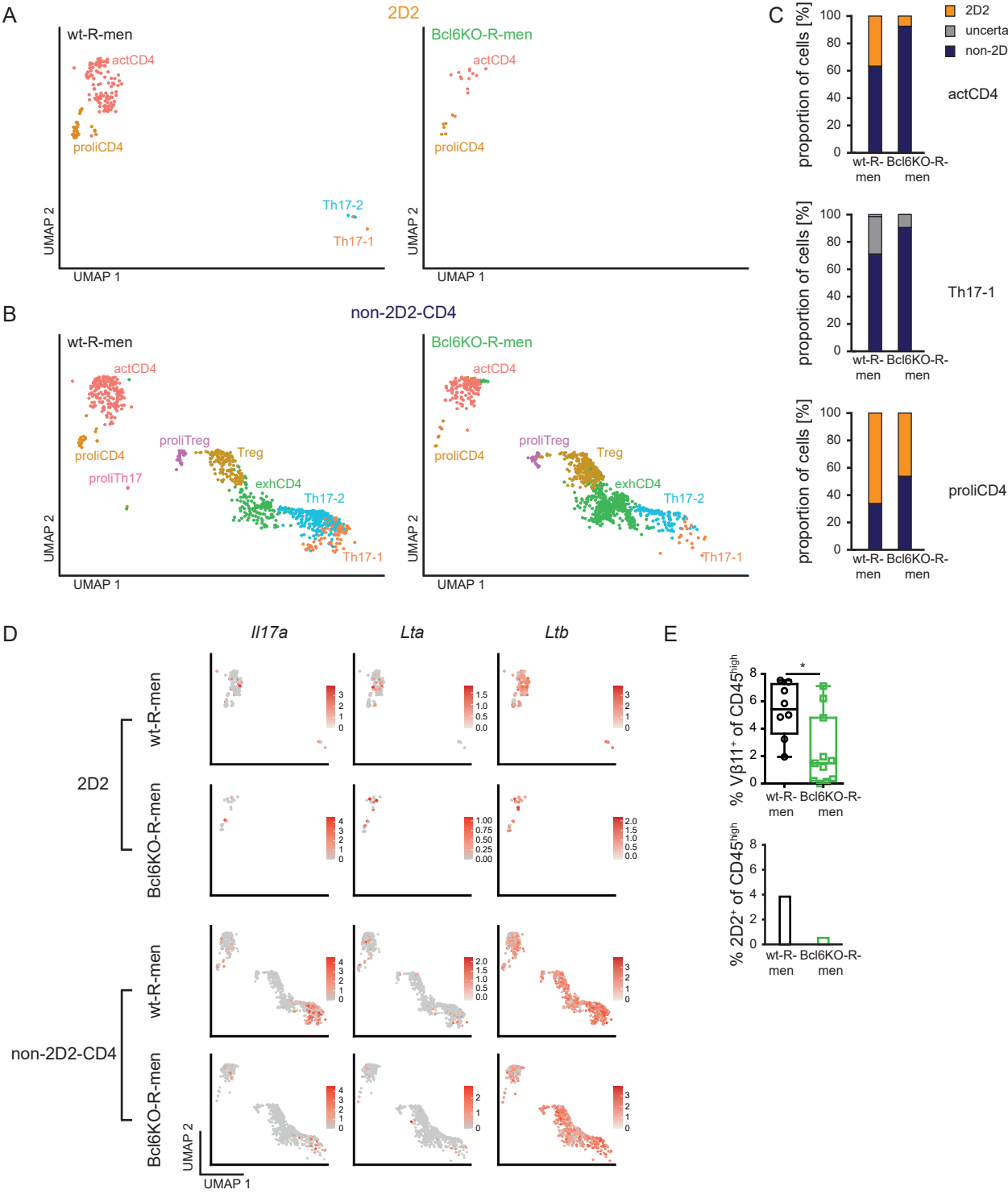
A
2D2
wt-R-men
actCD4
proliCD4
Th17-2
Th17-1
Bcl6KO-R-men
UMAP 2
UMAP 1
B
non-2D2-CD4
proliTreg
Treg
exhCD4
proliTh17
C
2D2
uncertain
non-2D2
proportion of cells [%]
actCD4
Th17-1
proliCD4
wt-R-men
Bcl6KO-R-men
D
Il17a
Lta
Ltb
2D2
non-2D2-CD4
E
% Vβ11+ of CD45high
% 2D2+ of CD45high
*

***Figure S7****: TCR sequencing identifies different proportions of donor-derived cells in the spinal cord meninges in wild type vs. Bcl6KO recipient mice.*

(A) Uniform Manifold Approximation and Projection (UMAP) plot with $CD4^+$ T cells expressing the $2D2^{tg}$ TCR in the meninges (men) of recipient (-R) mice of wild type (wt) or Bcl6KO $2D2^{tg}$ *in vitro* differentiated Th17 cells (wt-R (left) vs. Bcl6KO-R (right)). $2D2^{tg}$ TCR cells (2D2) were detected with TCR sequencing (Methods; Fig. S3E-I) from tissue-resident leukocytes isolated from SC meninges (men) at peak of disease of AT-EAE (experimental scheme in Fig. 1A and Fig. S5E). (B) UMAP plot of $CD4^+$ T cells expressing any non-$2D2^{tg}$ TCR in wt-R-men (left) and Bcl6KO-R-men (right). (C) Stacked bar-plots of the proportion of $2D2^{tg}$ TCR and non-$2D2^{tg}$ TCR within selected CD4 clusters (with a high proportion of cells expressing the $2D2^{tg}$ TCR) in wt-R-men vs. Bcl6KO-R-men is depicted. $CD4^+$ T cells were classified by single cell transcriptomes; $2D2^{tg}$ TCR $CD4^+$ T cells by the expression of the known $2D2^{tg}$ TCR α/β-sequence and a sufficient expression of the *Trac/Trbc* mRNA (Methods). (D) Feature plots of selected genes depicted in 2D2 (upper panels) and non-2D2 CD4 T cells (bottom panels) in wt-R-men and Bcl6KO-R-men. (E) Proportions of donor derived T cells of $CD45iv^{neg}CD45^{high}$ tissue-resident leukocytes (TRL) detected with flow cytometry ($V\beta11^+$ of $CD45^{high}$; upper panel) and TCR-sequencing related to all cells detected with scRNA-seq (bottom panel) in wt-R-men vs. Bcl6KO-R-men.

Abbreviations: AT-EAE *adoptive transfer experimental autoimmune encephalomyelitis, CD4* $CD4^+$ T cells, *act* activated, *proli* proliferating, *Treg* regulatory T cells, *exh* exhausted, *Th17* Th17 cells; *-R* recipient mice.

Figure S8

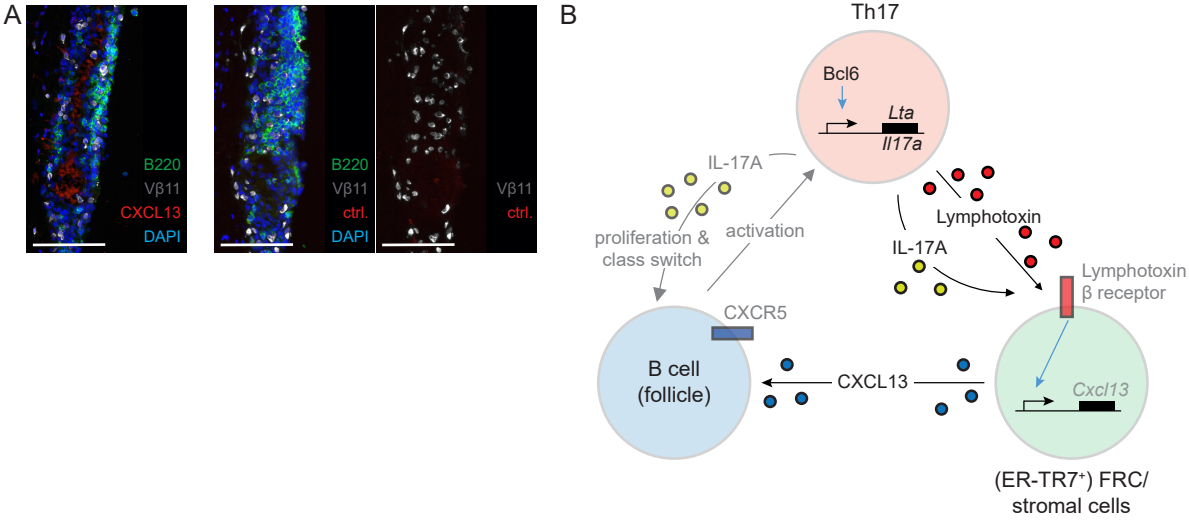
A
B220
Vβ11
CXCL13
DAPI
B220
Vβ11
ctrl.
DAPI
Vβ11
ctrl.
B
Th17
Bcl6
Lta
Il17a
IL-17A
proliferation &
class switch
activation
Lymphotoxin
IL-17A
Lymphotoxin
β receptor
CXCR5
B cell
(follicle)
CXCL13
Cxcl13
(ER-TR7+) FRC/
stromal cells

***Figure S8****: Bcl6-expressing Th17 cells can modulate a known local feed-forward loop in Th17 cells promoting meningeal neuroinflammation.*

(A) Secondary antibody control (ctrl) immunofluorescence staining (IF) for CXCL13 (Fig. 4D) of a spinal cord longitudinal section of a meningeal B cell aggregation in a representative wt-R at peak AT-EAE stained for the indicated markers (scale bars: 100 µm). (B) Scheme depicting potential interactions between encephalitogenic Th17 cells, follicular reticular cells (FRC)/stromal cells and follicular B cells in the meninges of AT-EAE recipient (wt-R-men) mice. We here integrate previous evidence (42, 43) and our data and hypothesize that the transcription factor Bcl6 promotes expression of Lymphotoxin-α and IL-17 in locally reactivated meningeal Th17 cells (Fig. 2C, H-J) which induces the production of B cell-supporting CXCL13 by meningeal stromal cells (42). Th17 cells were further shown to support B cell proliferation and class switch (43), in line with our data (Fig. 3F-H).

**Legends for Datasets S1-S26**

***Dataset S1****: Summary of technical information regarding samples and sequencing*
Technical information of all samples used for *single cell RNA-sequencing (scRNA-seq)*, single cell T cell receptor repertoire sequencing (Circularization *scTCR*) and bulk RNA-sequencing (*bulk RNA-seq*). Vβ11$^+$ wt-Th17 and Vβ11$^+$ Bcl6KO-Th17 samples are sorted Vβ11$^+$CD4$^+$ T cells from *in vitro* differentiated Th17 cells prior to intravenous injection for the induction of adoptive transfer (AT-) EAE. Vβ11$^+$ wt-R-par, Vβ11$^+$ Bcl6KO-R-par, Vβ11$^+$ wt-R-men and Vβ11$^+$ Bcl6KO-R-men samples are Vβ11$^+$CD4$^+$ T cells isolated from spinal cord meninges (men) or parenchyma (par) of wt or Bcl6KO AT-EAE recipient mice (wt-R or Bcl6KO-R). Abbreviations: *wt* wild type, *Bcl6KO* Bcl6 knockout, *men* meninges, *par* parenchyma, *Th17* Th17 cells.

***Dataset S2****: Top expressed genes defining 24 clusters in scRNA-seq of merged sample (wt-R-men, wt-R-par, Bcl6KO-R-men, Bcl6KO-R-par)*
Most frequently expressed genes (left) in all 24 clusters (right) identified in the first clustering performed with all cells (after doublet exclusion) from all four *scRNA-seq* samples (wt-R-men, wt-R-par, Bcl6KO-R-men, Bcl6KO-R-par). Avg_logFC: log fold change of the average expression. Pct.1: The percentage of cells where the gene is detected in group1. Pct.2: The percentage of cells where the gene is detected in group2. P_val_adj: Adjusted p-value, based on bonferroni correction using all genes in the dataset. Abbreviations: *scRNA seq* single cell RNA sequencing, *wt-R* wild type recipient, *Bcl6KO-R* Bcl6 knockout recipient, *men* meninges, *par* parenchyma, *Bc* B cells, *diffBc* differentiated B cells, *CD4* CD4$^+$ T cells, *act* activated, *Th17* Th17 cells, *Treg* regulatory T cells, *proli* proliferating, *exh* exhausted, *CD8* CD8$^+$ T cells, *CTL* cytotoxic T lymphocytes, *NK* natural killer cells, *prolicyt* proliferating cytotoxic T lymphocytes, *granulo* granulocytes, *micro* microglia, *DC* dendritic cells, *menDC* meningeal DC, *pDC* plasmacytoid DC, *cDC* classical DC, *myeloid* myeloid cells.

***Dataset S3****: Differentially expressed genes of scRNA-seq data of CD4 merged in wt-R-men vs. wt-R-par*
All clusters of scRNA-seq dataset identified as CD4 cells (Fig. 1B, Dataset S2,9, Fig. S2D; actCD4, proliCD4, proliTreg, Treg, exhCD4, Th17-1, Th17-2, proliTh17) were merged and most differentially expressed (DE) genes between wild type recipient (wt-R) meninges (men) and wt-R parenchyma (par) were calculated. Avg_logFC: log fold change of the average expression. Pct.1: The percentage of cells where the gene is detected in group1. Pct.2: The percentage of cells where the gene is detected in group2. P_val_adj: Adjusted p-value, based on bonferroni correction using all genes in the dataset. DE genes were calculated for all cell clusters with > 10 cells per sample. Abbreviations: *scRNA seq* single cell RNA sequencing, *wt-R* wild type recipient, *men* meninges, *par* parenchyma, *CD4* CD4$^+$ T cells, *act* activated, *proli* proliferating, *Treg* regulatory T cells, *exh* exhausted, *Th17* Th17 cells.

***Dataset S4****: Differentially expressed genes of scRNA-seq data of Th17 merged in wt-R-men vs. wt-R-par*
All clusters of scRNA-seq dataset identified as Th17 cells (Fig. 1B, Dataset S2,9, Fig. S2D; Th17-1, Th17-2, proliTh17) were merged and most differentially expressed (DE) genes between wild type recipient (wt-R) meninges (men) and wt-R parenchyma (par) were calculated. Avg_logFC: log fold change of the average expression. Pct.1: The percentage of cells where the gene is detected in group1. Pct.2: The percentage of cells where the gene is detected in group2. P_val_adj: Adjusted p-value, based on bonferroni correction using all genes in the dataset. DE genes were calculated for all cell clusters with > 10 cells per sample. Abbreviations: *scRNA seq* single cell RNA

sequencing, *wt-R* wild type recipient, *men* meninges, *par* parenchyma, *CD4* CD4$^+$ T cells, *proli* proliferating, *Th17* Th17 cells.

***Dataset S5****: Genes included in gene scores for Th17-1 and Th17 cell type identification*
Gene lists used for gene scores shown in Fig. S3C to identify Th17-1 like cells and Th17 like cells, respectively, in single cell RNA-sequencing datasets.

***Dataset S6:*** *Differentially expressed genes of bulk RNA-seq data of Vβ11$^+$ wt-R-men vs. Vβ11$^+$ wt-R-par*
Vβ11$^+$CD4$^+$ T cells isolated from spinal cord meninges (men) or parenchyma (par) of wt AT-EAE recipient (-R) mice were processed for bulk RNA seq. Differentially expressed (DE) genes from Vβ11$^+$ wt-R-men vs. Vβ11$^+$ wt-R-par are listed. BaseMean: The average of the normalized count values, dividing by size factors, taken over all samples. log2FoldChange: The effect size estimate, it indicates how much the gene or transcript's expression seems to have changed between the comparison and control groups. lfcSE: The standard error estimate for the log2 fold change estimate. Stat: The value of the test statistic for the gene or transcript. Pvalue: P-value of the test for the gene or transcript. Padj: Adjusted P-value for multiple testing for the gene or transcript (28). Abbreviations: *seq* sequencing, *wt* wild type, *-R* recipient, *men* meninges, *par* parenchyma.

***Dataset S7****: 2D2 TCR cells and non-2D2 cells in scRNA-seq clusters*
1) Cell numbers detected by scTCRseq data before filtering. Cell numbers and proportions of any TCR α chain, any TCR β chain, 2D2 TCR α chain, 2D2 TCR β chain in Total, CD4 T cells (CD4 T cells are the clusters of actCD4, proliCD4, proliTreg, Treg, exhCD4, Th17-1, Th17-2 and proliTh17) or proliferating and activated CD4 T cells (proliCD4, actCD4) among all samples, wt-R samples, or Bcl6KO-R samples (after doublet exclusion). All TCR chains were collected before filtering and identified by their occurrence in scRNA-seq data. 2) Confident 2D2 cells and non-2D2 & non-T cells detected by scTCR sequencing (Methods) in all 24 clusters of scRNA-seq of wt-R-men, wt-R-par, Bcl6KO-R-men and Bcl6KO-R-par samples. Confident 2D2 T cells and non-2D2 & non-T cells were filtered as in the method. 3) Percentage of confident 2D2 T cells in Total, CD4 T cells or proliCD4 and actCD4 among all samples, wt-R samples (wt-R-meninges [men] and wt-R-parenchyma [par] merged) or Bcl6KO-R (Bcl6KO-R-men and Bcl6KO-R-par merged) samples. Confident 2D2 T cells were filtered as in the method. Abbreviations: *scRNA seq* single cell RNA sequencing, *wt-R* wild type recipient, *Bcl6KO-R* Bcl6 knockout recipient, *men* meninges, *par* parenchyma, *Bc* B cells, *diffBc* differentiated B cells, *CD4* CD4$^+$ T cells, *act* activated, *Th17* Th17 cells, *Treg* regulatory T cells, *proli* proliferating, *exh* exhausted, *CD8* CD8$^+$ T cells, *CTL* cytotoxic T lymphocytes, *NK* natural killer cells, *prolicyt* proliferating cytotoxic T lymphocytes, *granulo* granulocytes, *micro* microglia, *DC* dendritic cells, *menDC* meningeal DC, *pDC* plasmacytoid DC, *cDC* classical DC, *myeloid* myeloid cells.

***Dataset S8****: Differentially expressed genes of 2D2 TCR cells vs. non-2D2 cells in merged CD4 T cell clusters in wt-R-men and wt-R-par merged*
Most differentially expressed (DE) genes in the merged CD4 T cell cluster (actCD4, proliCD4, proliTreg, Treg, exhCD4, Th17-1, Th17-2, proliTh17) in TCR sequencing data between 2D2-CD4 T cells and non-2D2-CD4 T cells in wt recipient samples (wt-R-men and wt-R-par). 2D2-CD4 T cells and non-2D2-CD4 T cells filtering rule was described in Methods. Avg_logFC: log fold change of the average expression. Pct.1: The percentage of cells where the gene is detected in group1. Pct.2: The percentage of cells where the gene is detected in group2. P_val_adj: Adjusted p-value, based on bonferroni correction using all genes in the dataset. DE genes were calculated by Seurat

(9) with default setting. Abbreviations: *CD4* CD4$^+$ T cells, *act* activated, *proli* proliferating, *Treg* regulatory T cells, *exh* exhausted, *Th17* Th17 cells, *TCR* T cell receptor.

***Dataset S9****: Cell number and percentage of 24 clusters and four cell lineages of four scRNA-seq samples*

At the peak of the AT-EAE an unbiased cell type clustering was performed from the meninges (men) and the parenchyma (par) of the wt and Bcl6KO recipients (wt-R and Bcl6KO-R). 24 individual cell clusters (left) were identified and annotated based on top expressed genes (Dataset S2) and predefined marker gene-sets (Fig. 2 SA-C). Cell numbers of the 24 clusters (column 2-5) and the percentage of the clusters (column 6-9) within each of the four samples (wt-R-men, wt-R-par, Bcl6KO-R-men, Bcl6KO-R-par) are listed. Clusters were classified into B cell (Bc), CD4$^+$ T cell (CD4), cytotoxic (cyto), and myeloid cell lineages (Fig. 1B). Percentages of each lineage are depicted for every sample. Abbreviations: *AT-EAE* adoptive transfer EAE, *scRNA seq* single cell RNA sequencing, *wt-R* wild type recipient, *Bcl6KO-R* Bcl6 knockout recipient, *men* meninges, *par* parenchyma, *Bc* B cells, *diffBc* differentiated B cells, *CD4* CD4$^+$ T cells, *act* activated, *Th17* Th17 cells, *Treg* regulatory T cells, *proli* proliferating, *exh* exhausted, *CD8* CD8$^+$ T cells, *CTL* cytotoxic T lymphocytes, *NK* natural killer cells, *prolicyt* proliferating cytotoxic T lymphocytes, *granulo* granulocytes, *micro* microglia, *DC* dendritic cells, *menDC* meningeal DC, *pDC* plasmacytoid DC, *cDC* classical DC, *myeloid* myeloid cells.

***Dataset S10****: Flow cytometry data in wt-R-men vs. wt-R-par*

Flow cytometry raw data from indicated populations in wt-R-men and wt-R-par as well as fold changes of selected cell populations between the indicated samples are depicted. Abbreviations: *wt-R* wild type recipient, *men* meninges, *par* parenchyma.

***Dataset S11****: Quantification of histology data – T cells, B cells, macrophages*

Histology quantification data from indicated populations in wt-R-men, wt-R-par, Bcl6KO-R-men and Bcl6KO-R-par. Values describe the density of cells within the indicated compartment (men, par) of the sample. Depicted are for CD3$^+$ and Vβ11$^+$ CD3$^+$ cells the cell density (cells / mm²) and for B220$^+$ and F4/80$^+$ cells the percentage of infiltrated area (% infiltrated area). Abbreviations: *wt-R* wild type recipient, *Bcl6KO-R* Bcl6 knockout recipient, *men* meninges, *par* parenchyma.

***Dataset S12****: Differentially expressed genes of bulk RNA-seq data of in vitro Vβ11$^+$ Bcl6KO-Th17 vs. Vβ11$^+$ wt-Th17*

Vβ11$^+$ wt-Th17 and Vβ11$^+$ Bcl6KO-Th17 samples are Vβ11$^+$CD4$^+$ T cells from *in vitro* differentiated Th17 cells prior to intravenous injection for the induction of adoptive transfer (AT-) EAE. Samples were processed for bulk RNA seq and differentially expressed (DE) genes from Vβ11$^+$ Bcl6KO-Th17 vs. Vβ11$^+$ wt-Th17 samples are listed. Abbreviations: *seq* sequencing, *wt* wildtype, *Bcl6KO* Bcl6 knockout, *Th17* Th17 cells, *seq* sequencing.

***Dataset S13****: Flow cytometry data in Bcl6KO-R-men vs. wt-R-men*

Flow cytometry raw data from indicated populations in wt-R-men and Bcl6KO-R-men as well as fold changes of selected cell populations between the indicated samples are depicted. Abbreviations: *wt-R* wild type recipient, *Bcl6KO-R* Bcl6 knockout recipient, *men* meninges.

***Dataset S14****: Flow cytometry data in Bcl6KO-R-par vs. wt-R-par*

Flow cytometry raw data from indicated populations in wt-R-par and Bcl6KO-R-par as well as fold changes of selected cell populations between the indicated samples are depicted. Abbreviations: *wt-R* wild type recipient, *Bcl6KO-R* Bcl6 knockout recipient, *par* parenchyma.

***Dataset S15:*** *Differentially expressed genes of bulk RNA-seq data of Vβ11⁺ Bcl6KO-R-par vs. Vβ11⁺ wt-R-par*

Vβ11⁺CD4⁺ T cells isolated from spinal cord parenchyma (par) of wt or Bcl6KO AT-EAE recipient (-R) mice were processed for bulk RNA seq. Differentially expressed (DE) genes from Vβ11⁺ Bcl6KO-R-par vs. Vβ11⁺ wt-R-par are listed. Abbreviations: *seq* sequencing, *wt* wild type, *Bcl6KO* Bcl6 knockout, *-R* recipient, *par* parenchyma.

***Dataset S16:*** *Differentially expressed genes of bulk RNA-seq data of Vβ11⁺ Bcl6KO-R-men vs. Vβ11⁺ wt-R-men*

Vβ11⁺CD4⁺ T cells isolated from spinal cord meninges (men) of wt or Bcl6KO AT-EAE recipient (-R) mice were processed for bulk RNA seq. Differentially expressed (DE) genes from Vβ11⁺ Bcl6KO-R-men vs. Vβ11⁺ wt-R-men are listed. Abbreviations: *seq* sequencing, *wt* wild type, *Bcl6KO* Bcl6 knockout, *-R* recipient, *men* meninges.

***Dataset S17****: Differentially expressed genes of scRNA-seq data of merged B cells in Bcl6KO-R-men vs. wt-R-men*

Most differentially expressed (DE) genes in the merged Bc cluster (Fig. 3, Dataset S2,9, Fig. S2D) in scRNA seq data between Bcl6KO-R-men vs wt-R-men. Avg_logFC: log fold change of the average expression. Pct.1: The percentage of cells where the gene is detected in group1. Pct.2: The percentage of cells where the gene is detected in group2. P_val_adj: Adjusted p-value, based on bonferroni correction using all genes in the dataset. Abbreviations: *scRNA seq* single cell RNA sequencing, *wt-R* wild type recipient, *Bcl6KO-R* Bcl6 knockout recipient, *men* meninges, *par* parenchyma, *Bc* B cells, *diffBc* differentiated B cells.

***Dataset S18****: Marker genes of five B cell subclusters in scRNA-seq data in Bcl6KO-R-men and wt-R-men*

Most frequently expressed genes in the five Bc subclusters (Bc1, Bc2, Bc3, FOBc, PC) in Bcl6KO-R-men and wt-R-men are listed. All cells identified as B cells in scRNA-seq data in Bcl6KO-R-men and wt-men-R were merged (Fig. 1B, Dataset S2,9, Fig. S2D) and then sub-clustered with higher resolution. Avg_logFC: log fold change of the average expression. Pct.1: The percentage of cells where the gene is detected in group1. Pct.2: The percentage of cells where the gene is detected in group2. P_val_adj: Adjusted p-value, based on bonferroni correction using all genes in the dataset. Abbreviations: *scRNA seq* single cell RNA sequencing, *wt-R* wild type recipient, *Bcl6KO-R* Bcl6 knockout recipient, *men* meninges, *par* parenchyma, *Bc* B cells, *FOBc* follicular B cells, *PC* plasma cells.

***Dataset S19****: Cluster size of five Bc subclusters in scRNA-seq data in Bcl6KO-R-men and wt-R-men*

A sub-clustering was performed from all meningeal B cell transcriptomes in scRNA-seq data and five B cell sub-clusters were identified (*Bc1, Bc2, Bc3, FOBc, PC* - left). Cell number in the five clusters (column 2+3) and the proportion of the clusters (column 4+5) within each of the two meninges samples (wt-R-men, Bcl6KO-R-men) are listed. Abbreviations: *scRNA seq* single cell RNA sequencing, *wt-R* wild type recipient, *Bcl6KO-R* Bcl6 knockout recipient, *men* meninges, *par* parenchyma, *Bc* B cells, *FOBc* follicular B cells, *PC* plasma cells.

***Dataset S20****: Detailed results of immunoglobulin isotype concentrations measured in cerebrospinal fluid (CSF)*

Detailed results of immunoglobulin (Ig) isotype concentrations in the cerebrospinal fluid (CSF) measured by ThermoFisher (Invitrogen) Antibody Isotyping 7-Plex Mouse ProcartaPlex Panel

(Methods) are depicted. CSF was taken at the peak of AT-EAE of sick wt and Bcl6KO recipients (wt-R and Bcl6KO-R). Dataset contains the exact concentrations per mouse of differentially abundant immunoglobulin isotypes (Fig. 3F) in wt-R and Bcl6KO-R and the volume of isolated CSF. Abbreviations: *AT-EAE* adoptive transfer EAE, *wt* wildtype, *Bcl6KO* Bcl6 knockout, *-R* recipient.

***Dataset S21****: Quantification of histology data – Ki67⁺ B220⁺ cells.*
Histology quantification data from indicated populations in wt-R-men, wt-R-par, Bcl6KO-R-men and Bcl6KO-R-par. Values describe the density of cells within the indicated compartment (men, par) of the sample. Depicted is the cell density of $Ki67^+$ $B220^+$ cells (cells / $mm^2$). Abbreviations: *wt-R* wild type recipient, *Bcl6KO-R* Bcl6 knockout recipient, *men* meninges, *par* parenchyma.

***Dataset S22****: Detailed results of chemokines measured in cerebrospinal fluid (CSF)*
Detailed results of cerebrospinal fluid (CSF) proteomics measured by Bio-Plex Pro mouse chemokine panel 31-plex (Methods) are depicted. CSF was taken at the peak of AT-EAE of sick wt and Bcl6KO recipients (wt-R and Bcl6KO-R). Dataset contains names of cytokines that were screened and the exact concentrations per mouse of differentially abundant cytokines (Fig. 4A) in wt-R and Bcl6KO-R. Abbreviations: *AT-EAE* adoptive transfer EAE, *wt* wildtype, *Bcl6KO* Bcl6 knockout, *-R* recipient.

***Dataset S23****: TCR Sequencing Primers and 4 steps PCR program*
Technical information of T cell receptor (TCR) sequencing. TCR, T cell receptor. “R”, a purine base (arginine (A) or guanine (G)). “Y”, a pyrimidine base (cytosine (C) or thymidine (T)). “B”, a base of either C, G or T. 4 step PCR was used in TCR Repertoire enrichment. 2 annealing steps (63° C and 57 °C) were used due to the annealing temperatures’ difference between PolyA primer and TCR rev primers. Temperature was defined with degrees celsius (°C) and duration time in hh:mm:ss.

***Dataset S24****: Differentially expressed genes of scRNA-seq data of all 24 clusters in wt-R-men vs. wt-R-par*
Differentially expressed (DE) genes between wild type recipients (wt-R) meninges (men) and wt-R parenchyma (par) in scRNA seq data were calculated. Avg_logFC: log fold change of the average expression. Pct.1: The percentage of cells where the gene is detected in group1. Pct.2: The percentage of cells where the gene is detected in group2. P_val_adj: Adjusted p-value, based on bonferroni correction using all genes in the dataset. DE genes were calculated for all cell clusters with > 10 cells per sample.
Abbreviations: *scRNA seq* single cell RNA sequencing, *wt-R* wild type recipient, *men* meninges, *par* parenchyma.

***Dataset S25****: Differentially expressed genes of scRNA-seq data of all 24 clusters in Bcl6KO-R-men vs. wt-R-men*
Differentially expressed (DE) genes between Bcl6KO (Bcl6 knockout) recipients (Bcl6KO-R) meninges (men) and wild type recipients (wt-R) men in scRNA seq data were calculated. Avg_logFC: log fold change of the average expression. Pct.1: The percentage of cells where the gene is detected in group1. Pct.2: The percentage of cells where the gene is detected in group2. P_val_adj: Adjusted p-value, based on bonferroni correction using all genes in the dataset. DE genes were calculated for all cell clusters with > 10 cells per sample.
Abbreviations: *scRNA seq* single cell RNA sequencing, *wt* wild type, *Bcl6KO* Bcl6 knockout, *-R* recipients, *men* meninges.

***Dataset S26****: Differentially expressed genes of scRNA-seq data of all 24 clusters in Bcl6KO-R-par vs. wt-R-par*

Differentially expressed (DE) genes between Bcl6KO (Bcl6 knockout) recipients (Bcl6KO-R) parenchyma (par) and wild type recipients (wt-R) par in scRNA seq data were calculated. Avg_logFC: log fold change of the average expression. Pct.1: The percentage of cells where the gene is detected in group1. Pct.2: The percentage of cells where the gene is detected in group2. P_val_adj: Adjusted p-value, based on bonferroni correction using all genes in the dataset. DE genes were calculated for all cell clusters with > 10 cells per sample.

Abbreviations: *scRNA seq* single cell RNA sequencing, *wt* wild type, *Bcl6KO* Bcl6 knockout, *-R* recipients, *par* parenchyma.

**SI References**


1. P. P. Lee, *et al.*, A critical role for Dnmt1 and DNA methylation in T cell development, function, and survival. *Immunity* **15**, 763–774 (2001).

2. E. Bettelli, *et al.*, Myelin oligodendrocyte glycoprotein-specific T cell receptor transgenic mice develop spontaneous autoimmune optic neuritis. *J. Exp. Med.* **197**, 1073–1081 (2003).

3. K. Hollister, *et al.*, Insights into the role of Bcl6 in follicular Th cells using a new conditional mutant mouse model. *J. Immunol.* **191**, 3705–3711 (2013).

4. D. Schafflick, *et al.*, Integrated single cell analysis of blood and cerebrospinal fluid leukocytes in multiple sclerosis. *Nat. Commun.* **11**, 247 (2020).

5. T. Litzenburger, *et al.*, B lymphocytes producing demyelinating autoantibodies: development and function in gene-targeted transgenic mice. *J. Exp. Med.* **188**, 169–180 (1998).

6. Fas Promotes T Helper 17 Cell Differentiation and Inhibits T Helper 1 Cell Development by Binding and Sequestering Transcription Factor STAT1. - PubMed - NCBI (June 6, 2018).

7. S. J. Guyenet, *et al.*, A simple composite phenotype scoring system for evaluating mouse models of cerebellar ataxia. *J. Vis. Exp.* (2010) https:/doi.org/10.3791/1787.

8. E. M. Steinert, *et al.*, Quantifying Memory CD8 T Cells Reveals Regionalization of Immunosurveillance. *Cell* **161**, 737–749 (2015).

9. T. Stuart, *et al.*, Comprehensive Integration of Single-Cell Data. *Cell* **177**, 1888–1902.e21 (2019).

10. J. Wolbert, *et al.*, Redefining the heterogeneity of peripheral nerve cells in health and autoimmunity. *Proc. Natl. Acad. Sci. U. S. A.* (2020) https:/doi.org/10.1073/pnas.1912139117.

11. E. A. K. DePasquale, *et al.*, DoubletDecon: Deconvoluting Doublets from Single-Cell RNA-Sequencing Data. *Cell Rep.* **29**, 1718–1727.e8 (2019).

12. C. Hafemeister, R. Satija, Normalization and variance stabilization of single-cell RNA-seq data using regularized negative binomial regression. *bioRxiv*, 576827 (2019).

13. K. Blighe, *EnhancedVolcano* (Bioconductor, 2018) https:/doi.org/10.18129/B9.BIOC.ENHANCEDVOLCANO.

14. M. Singh, *et al.*, High-throughput targeted long-read single cell sequencing reveals the clonal and transcriptional landscape of lymphocytes. *Nat. Commun.* **10**, 3120 (2019).

15. M.-P. Lefranc, *et al.*, IMGT®, the international ImMunoGeneTics information system® 25 years on. *Nucleic Acids Res.* **43**, D413–22 (2015).

16. M. Heming, *et al.*, Neurological Manifestations of COVID-19 Feature T Cell Exhaustion and Dedifferentiated Monocytes in Cerebrospinal Fluid. *Immunity* **54**, 164–175.e6 (2021).

17. A. M. Klein, *et al.*, Droplet barcoding for single-cell transcriptomics applied to embryonic stem cells. *Cell* **161**, 1187–1201 (2015).

18. E. Z. Macosko, *et al.*, Highly Parallel Genome-wide Expression Profiling of Individual Cells Using Nanoliter Droplets. *Cell* **161**, 1202–1214 (2015).

19. E. Azizi, *et al.*, Single-Cell Map of Diverse Immune Phenotypes in the Breast Tumor Microenvironment. *Cell* **174**, 1293–1308.e36 (2018).

20. W. Shen, S. Le, Y. Li, F. Hu, SeqKit: A Cross-Platform and Ultrafast Toolkit for FASTA/Q File Manipulation. *PLoS One* **11**, e0163962 (2016).

21. L. E. Lucca, *et al.*, Bispecificity for myelin and neuronal self-antigens is a common feature of CD4 T cells in C57BL/6 mice. *J. Immunol.* **193**, 3267–3277 (2014).

22. E. Bettelli, *et al.*, Reciprocal developmental pathways for the generation of pathogenic effector TH17 and regulatory T cells. *Nature* **441**, 235–238 (2006).

23. S. Picelli, *et al.*, Smart-seq2 for sensitive full-length transcriptome profiling in single cells. *Nat. Methods* **10**, 1096–1098 (2013).

24. A. M. Bolger, M. Lohse, B. Usadel, Trimmomatic: a flexible trimmer for Illumina sequence data. *Bioinformatics* **30**, 2114–2120 (2014).

25. D. Kim, B. Langmead, S. L. Salzberg, HISAT: a fast spliced aligner with low memory requirements. *Nat. Methods* **12**, 357–360 (2015).

26. H. Li, *et al.*, The Sequence Alignment/Map format and SAMtools. *Bioinformatics* **25**, 2078–2079 (2009).

27. S. Anders, P. T. Pyl, W. Huber, HTSeq--a Python framework to work with high-throughput sequencing data. *Bioinformatics* **31**, 166–169 (2015).

28. M. I. Love, W. Huber, S. Anders, Moderated estimation of fold change and dispersion for RNA-seq data with DESeq2. *Genome Biol.* **15**, 550 (2014).

29. V. Narayanan, *et al.*, Impairment of frequency-specific responses associated with altered electrical activity patterns in auditory thalamus following focal and general demyelination. *Exp. Neurol.* **309**, 54–66 (2018).

30. L. Liu, K. Duff, A technique for serial collection of cerebrospinal fluid from the cisterna magna in mouse. *J. Vis. Exp.* (2008) https:/doi.org/10.3791/960.

31. N. K.-H. Lim, *et al.*, An Improved Method for Collection of Cerebrospinal Fluid from Anesthetized Mice. *J. Vis. Exp.* (2018) https:/doi.org/10.3791/56774.

32. C. R. Parker Harp, *et al.*, Neutrophils promote VLA-4-dependent B cell antigen presentation and accumulation within the meninges during neuroinflammation. *Proc. Natl. Acad. Sci. U. S. A.* **116**, 24221–24230 (2019).

33. A. Louveau, A. J. Filiano, J. Kipnis, Meningeal whole mount preparation and characterization of neural cells by flow cytometry. *Curr. Protoc. Immunol.* **121** (2018).

34. A. Louveau, *et al.*, Structural and functional features of central nervous system lymphatic vessels. *Nature* **523**, 337–341 (2015).

35. H. Gerwien, *et al.*, Imaging matrix metalloproteinase activity in multiple sclerosis as a specific marker of leukocyte penetration of the blood-brain barrier. *Sci. Transl. Med.* **8**, 364ra152 (2016).

36. S. Agrawal, *et al.*, Dystroglycan is selectively cleaved at the parenchymal basement membrane at sites of leukocyte extravasation in experimental autoimmune encephalomyelitis. *J. Exp. Med.* **203**, 1007–1019 (2006).

37. S. J. Ralph, M. V. Berridge, Expression of antigens of the'T200'family of glycoproteins on hemopoietic stem cells: evidence that thymocyte cell lineage antigens are represented on'T200'. *The Journal of Immunology* **132**, 2510–2514 (1984).

38. L. M. Sorokin, *et al.*, Developmental Regulation of the Laminin α5 Chain Suggests a Role in Epithelial and Endothelial Cell Maturation. *Dev. Biol.* **189**, 285–300 (1997).

39. H. Van Hove, *et al.*, A single-cell atlas of mouse brain macrophages reveals unique transcriptional identities shaped by ontogeny and tissue environment. *Nat. Neurosci.* **22**, 1021–1035 (2019).

40. M. J. C. Jordão, *et al.*, Single-cell profiling identifies myeloid cell subsets with distinct fates during neuroinflammation. *Science* **363** (2019).

41. A. Jager, V. Dardalhon, R. A. Sobel, E. Bettelli, V. K. Kuchroo, Th1, Th17, and Th9 effector cells induce experimental autoimmune encephalomyelitis with different pathological phenotypes. *J. Immunol.* **183**, 7169–7177 (2009).

42. N. B. Pikor, *et al.*, Integration of Th17- and Lymphotoxin-Derived Signals Initiates Meningeal-Resident Stromal Cell Remodeling to Propagate Neuroinflammation. *Immunity* **43**, 1160–1173 (2015).

43. M. Mitsdoerffer, *et al.*, Proinflammatory T helper type 17 cells are effective B-cell helpers. *Proc. Natl. Acad. Sci. U. S. A.* **107**, 14292–14297 (2010).